AD-A131 546 NUCLEAR MOMENT ALIGNMENT RELAXATION AND DETECTION MECHANISMS(U) LITTON SYSTEMS INC WOODLAND HILLS CA GUIDANCE AND CONTROL SYS... A T NICOL ET AL. MAR 83 1/1

UNCLASSIFIED 404720 AFOSR-TR-83-0622 F49620-82-C-0047 F/G 20/8 NL

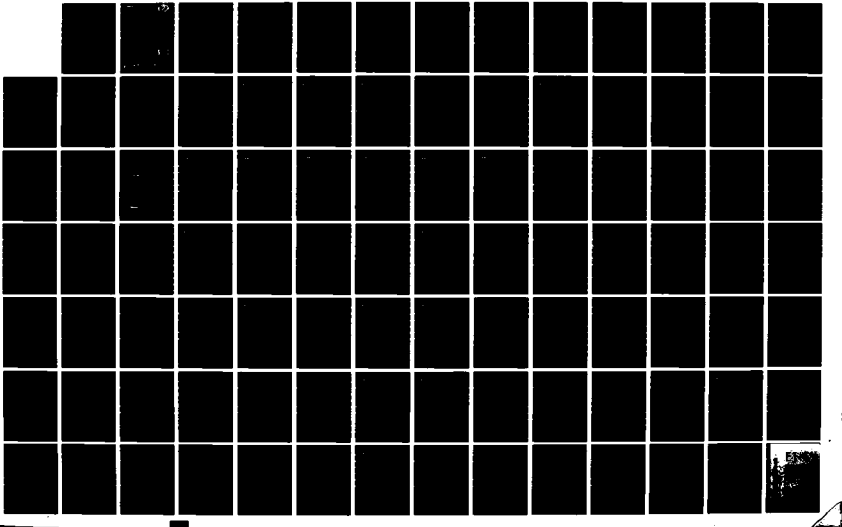

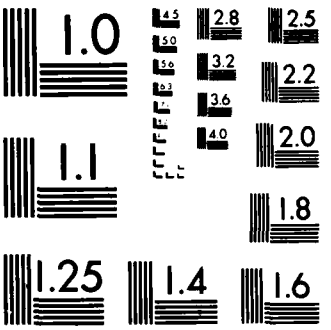

AFOSR-TR- 83-0622
Document No. 405039
March 1983

NUCLEAR MOMENT ALIGNMENT, RELAXATION AND DETECTION MECHANISMS

March 1982 - February 1983

FINAL TECHNICAL REPORT

Contract No. F49620-82-C-0047

Prepared for
AIR FORCE OFFICE OF SCIENTIFIC RESEARCH

Litton GUIDANCE & CONTROL SYSTEMS
5500 Canoga Avenue, Woodland Hills, California 91365

Document No. 405039
March 1983

NUCLEAR MOMENT ALIGNMENT, RELAXATION AND DETECTION MECHANISMS

March 1982 - February 1983

FINAL TECHNICAL REPORT

Prepared for

AIR FORCE OFFICE OF SCIENTIFIC RESEARCH

Under

Contract No. F49620-82-C-0047

Approved By:

Edward Phillips
Manager, NMR Gyro Project

Litton GUIDANCE & CONTROL SYSTEMS
5500 Canoga Avenue, Woodland Hills, California 91365

UNCLASSIFIED

SECURITY CLASSIFICATION OF THIS PAGE (When Data Entered)

REPORT DOCUMENTATION PAGE

READ INSTRUCTIONS BEFORE COMPLETING FORM

1. REPORT NUMBER: AFOSR-TR- 83-0622	2. GOVT ACCESSION NO.: AD-A131546
3. RECIPIENT'S CATALOG NUMBER:	
4. TITLE (and Subtitle): NUCLEAR MOMENT ALIGNMENT, RELAXATION AND DETECTION MECHANISMS	5. TYPE OF REPORT & PERIOD COVERED: Final (March 1982- February 1983)
	6. PERFORMING ORG. REPORT NUMBER: 404720
7. AUTHOR(s): A.T. NICOL, L. LAM, W. BOLEY	8. CONTRACT OR GRANT NUMBER(s): F49620-82-C-0047
9. PERFORMING ORGANIZATION NAME AND ADDRESS: Litton Guidance & Control Systems, 5500 Canoga Ave., Woodland Hills, CA 91365	10. PROGRAM ELEMENT, PROJECT, TASK AREA & WORK UNIT NUMBERS: 61102F / 2301/A4
11. CONTROLLING OFFICE NAME AND ADDRESS: Director of Physics Code FQ 8671, Air Force Office of Scientific Research, Attn: NP Building 410, Bolling AFB, D.C. 20332	12. REPORT DATE: March 1983
	13. NUMBER OF PAGES: 92
14. MONITORING AGENCY NAME & ADDRESS(if different from Controlling Office): Same	15. SECURITY CLASS. (of this report): UNCLASSIFIED
	15a. DECLASSIFICATION/DOWNGRADING SCHEDULE

16. DISTRIBUTION STATEMENT (of this Report)

Approved for public release; distribution unlimited.

17. DISTRIBUTION STATEMENT (of the abstract entered in Block 20, if different from Report)

18. SUPPLEMENTARY NOTES

19. KEY WORDS (Continue on reverse side if necessary and identify by block number)

Nuclear Magnetic Resonance	Nuclear Moment Relaxation	Frequency Shift
Gyroscope	Quadrupole Relaxation	
Optical Pumping	Nuclear Moment Precession	
Nuclear Moment Alignment	Spin Exchange	

20. ABSTRACT (Continue on reverse side if necessary and identify by block number)

The reported physics research is part of an overall program to develop a nuclear magnetic resonance gyro that makes use of an optically pumped alkali metal vapor both to align the magnetic moments of the noble gas nuclei and to detect the weak magnetic fields that are generated by these precessing nuclear moments.

DD FORM 1 JAN 73 1473 EDITION OF 1 NOV 65 IS OBSOLETE

UNCLASSIFIED

SECURITY CLASSIFICATION OF THIS PAGE (When Data Entered)

20. ABSTRACT (cont)

A model for the distribution of polarization of optically pumped rubidium across a sample cell is developed. Results of the computer modeling are presented graphically for various cells as a function of cell size, incident light intensity, wall type and gas fill.

A study of the effect of direct nuclear dipole-dipole interaction on surface relaxation of ^{129}Xe is reported. Results indicate that the mechanism for ^{129}Xe nuclear relaxation on surfaces studied is not the direct dipolar interaction and must be attributed to an electron-nucleus interaction.

Studies of ^{129}Xe relaxation on several surface types show an order of magnitude more efficient relaxation of ^{129}Xe on plain pyrex as compared with rubidium hydride surfaces. Rubidium hydride surfaces are found to be about a factor of three more efficient than silicone treated surfaces for relaxing xenon nuclear spins.

Studies of mixed alkali rubidium-cesium NMR cells show that in such systems a relatively short ^{129}Xe pump time can be achieved at a relatively low temperature as compared with cells containing only rubidium. Furthermore, it is shown experimentally that the mixed alkali-^{129}Xe system has approximately the same effective spin exchange cross section as the single alkali-xenon system.

A rate equation model to calculate $\langle S_z \rangle$ with narrow band pumping is presented, and preliminary experiments using a laser diode source for off resonance optical pumping are discussed.

GUIDANCE & CONTROL SYSTEMS
5500 Canoga Avenue, Woodland Hills, California 91365

FSCM 06481

TABLE OF CONTENTS

GUIDANCE & CONTROL SYSTEMS
5500 Canoga Avenue, Woodland Hills, California 91365

TABLE OF CONTENTS (cont)

GUIDANCE & CONTROL SYSTEMS
5500 Canoga Avenue, Woodland Hills, California 91365

FSCM 06481

TABLE OF CONTENTS (cont)

GUIDANCE & CONTROL SYSTEMS
5500 Canoga Avenue, Woodland Hills, California 91365

FSCM 06481

LIST OF ILLUSTRATIONS

GUIDANCE & CONTROL SYSTEMS
5500 Canoga Avenue, Woodland Hills, California 91365

FSCM 06481

LIST OF TABLES

GUIDANCE & CONTROL SYSTEMS
Litton 5500 Canoga Avenue, Woodland Hills, California 91365

FSCM 06481

SECTION I

PROGRAM DESCRIPTION

1.1 INTRODUCTION

For several years Litton Guidance and Control Systems has been involved in a research and development effort aimed at perfecting a nuclear magnetic resonance gyro (NMRG). The nuclear magnetic resonance gyro is based on the principle that a nuclear moment, when placed in a magnetic field, will precess with a characteristic frequency about the field direction. In the event that the apparatus is itself rotated about the field direction there will be an apparent change in the precession frequency which can be directly related to the rotation of the device. In order to avoid the necessity of maintaining an extremely precise magnetic field strength the current demonstration model gyro (DMG) uses two isotopes of xenon, each with a well known nuclear moment. Each moment has a characteristic gyromagnetic ratio and the relative precession frequencies remain constant; hence, the physical rotation of the device can be obtained without precise knowledge of the field strength.

In the Litton gyro the nuclear polarization is achieved through a spin exchange process with optically pumped rubidium vapor. Important to the successful development of the NMR gyro is the ability to produce a high long-lived polarization of the noble gas nuclei. As the alkali metal-noble gas systems are contained in small glass cells of about 1 ml volume, both surface and gas phase effects are important in achieving and maintaining the desired nuclear polarization. The AFOSR sponsored research addresses these questions.

GUIDANCE & CONTROL SYSTEMS
Litton 5500 Canoga Avenue, Woodland Hills, California 91365

1.2 OBJECTIVES AND STATUS OF THE PROGRAM

In the project year 1982-83 four areas of research were proposed. The first of these was a modeling of ribidium polarization distribution across a sample cell followed by related experiments. The results of this study are presented in Section II. The model predicts rubidium polarization distribution within a sample cell for various sets of parameters such as xenon and buffer gas pressures, incident light intensity and cell size. The model successfully predicts a minimum of rubidium polarization gradier for the standard DMG cell in the research apparatus or in the act gyro, and related experiments confirm this prediction. The model is being used to judge the importance of cell parameters such as cell size and buffer gas pressure in gyro cell design. Related experiments are reported.

The second research area concerned an investigation of non-RbH cell boundaries. A detailed study of RbD versus RbH surfaces confirmed the wall relaxation mechanism for ^{129}Xe to be due to an electron-nuclear interaction rather than a direct dipolar nuclear-nuclear interaction. The RbD/RbH study is reported in Section III. In Section IV studies of comparisons of several different surfaces are presented. The studies presented in Sections III and IV are being prepared for publication.

The third area of research involved studies of a mixed alkali-^{129}Xe system. The results, presented in Section V, demonstrate that an unusually fast Xe pump up time can be achieved at ~80C using a rubidium-cesium mixture. The results also confirm that the mixed alkali-^{129}Xe system has approximately the same effective spin exchange cross section as the single alkali-^{129}Xe system.

Finally, as reported in Section VI, studies of off resonance optical pumping were carried out. These studies include a theoretical prediction of the xenon nuclear polarization which can be

achieved using a narrow band source such as a laser diode and a discussion of experimental results.

1.3 PROFESSIONAL PERSONNEL ASSOCIATED WITH PROGRAM

The principal investigator for this program has been Dr. Ann T. Nicol who, in addition to coordinating the overall research program, devised and carried out cell surface studies and studies related to rubidium polarization effects. Mr. Wm. Boley performed the actual modeling of rubidium polarization effects with assistance from Dr. George Kamin. Dr. Leo Lam was responsible for the mixed alkali study and for the off resonance optical pumping experiments. Mr. James Eddingfield maintained the research apparatus and was responsible for taking many data. Data were also taken by Mr. J. Vallino, Jr. All cells were prepared by Mr. Wm. Debley. Dr. Nicol is especially pleased to acknowledge extremely useful discussions with Dr. Edward Kaneysberg.

Dr. A. T. Nicol presented a seminar entitled "Xenon NMR in Very Low Magnetic Fields" on February 4, 1983 at the University of Delaware. Material presented in Sections II, III and IV was discussed.

GUIDANCE & CONTROL SYSTEMS
Litton 5500 Canoga Avenue, Woodland Hills, California 91365

FSCM 06481

SECTION II

SPACIAL DISTRIBUTION OF POLARIZATION OF OPTICALLY PUMPED RUBIDIUM

2.1 INTRODUCTION

The question of the spacial distribution of alkali metal polarization in optical pumping experiments is an important one which has been specifically addressed in the case of cesium (Ref 2-1). It is important to characterize the effects of diffusion on spacial distribution of polarization of optically pumped species thereby taking into consideration the effects of the cell buffer gas pressures. In addition, alkali metal atom polarization is affected by any spin exchange interactions and depends on pressures of atoms containing nuclear spin such as ^{129}Xe (spin 1/2). Furthermore, the wall of the vessel is more or less depolarizing; thus a sharp polarization gradient can occur at the surface. Depending on the effects of diffusion and of light intensity there is a possibility that a non-uniform polarization distribution will exist across the sample cell. The alkali non-uniform metal polarization distribution is experienced as a magnetic field gradient by the noble gas nuclei having the spin and is a source of relaxation. The effect has been demonstrated experimentally (Ref 2-2). In order to evaluate the importance of this effect, a computer modeling of the problem was undertaken in which the rubidium-xenon-buffer gas system was considered.

Before discussing the factors involved in polarization of rubidium in a glass cell, some background on a particular application is provided. The primary use of the cell containing rubidium is in the Nuclear Magnetic Resonance (NMR) Gyroscope. The NMR gyro operates on the principle of sensing inertia angular rotation rates as a shift in the Larmor precession frequency of one or more nuclear species that possess nuclear magnetic moments. The Larmor

precession frequency is the frequency with which a magnetic moment will precess about the direction of a magnetic field. In the particular case addressed here, two different noble gas isotopes are used as the magnetic moment species. These are combined with an alkali metal vapor in a glass cell which is then placed in a controlled magnetic field environment. In the Demonstration Model Gyro (DMG) the cell is illuminated by two beams of light that are generated by an alkali metal vapor RF discharge lamp containing the same type of alkali metal that is used in the cell. One of the beams is circularly polarized and is used for magnetic moment alignment. The other beam is plane polarized and is used for detection. The detection beam is placed orthogonal to the circularly polarized light beam and after passing through the cell is sensed by a photodetector. The output signal from the photodetector is processed to produce information concerning the rotation rate of the gyroscope. In order to study cell characteristics a research apparatus requiring only one circularly polarized beam is used. To characterize effects due to the presence of any external field inhomogeneities, i.e., rubidium polarization inhomogeneities, several types of experiments are carried out using the research apparatus. Those types of experiments were thoroughly discussed and the research apparatus described in a previous report (Ref 2-2).

This study considers the processes that take place in the cell containing the alkali metal, in particular, rubidium. The atomic magnetic moments of the rubidium metal atoms are partially aligned in the direction of the incident light by absorption of some of the light in an optical pumping process. The nuclear magnetic moments of the noble gas atoms, in this study two isotopes of xenon, are also partially aligned through a spin exchange mechanism during collision with the aligned alkali metal atom. The alignment of atoms with the magnetic field is termed polarization.

This study is aimed at finding the spacial distribution of the rubidium polarization. With spacial distribution information, the effects of changing light intensity on the system can be more accurately determined and it becomes possible to predict an optimum light level for gyro operation. Also the study of the effects of using different cell geometries should lead to predictions of the shape of a cell which can produce better performance without having to construct and test different cell shapes. A better description of the polarization can lead to a better mathematical description of gyro operation. Through a simulation it is possible to change many parameters of the system and obtain results which predict performance more quickly than by running laboratory experiments. This is particularly important inasmuch as preparing and testing a wide variety of cells is extremely time consuming. This study looks at the effects of changing lamp intensity, and the shape of the cell as well as gas fill. The resulting graphs of the rubidium polarization distribution in the cell as a function of light intensity, cell size and cell shape permit comparison with experimental results. The theory of optical pumping, thoroughly described in the literature (Ref 2-3), is based on the use of quantum mechanics for its mathematical models. The approach used here is to use partial differential equations (PDE) and describe the observed phenomenon as a field problem (Ref 2-4). The results of quantum mechanics are used to arrive at the parameters for the model.

2.2 MATHEMATICAL MODEL

The system under investigation is shown schematically in figure 2-1. The cell containing the rubidium and xenon gases is irradiated with circularly polarized light while a photo-diode detects the absorption of the cell. A magnetic field (pump field) is also applied to the cell in the same direction as the incoming light. The light source is a rubidium lamp and emits light at the proper frequencies for absorption by the cell.

GUIDANCE & CONTROL SYSTEMS
5500 Canoga Avenue, Woodland Hills, California 91365

FSCM 06481

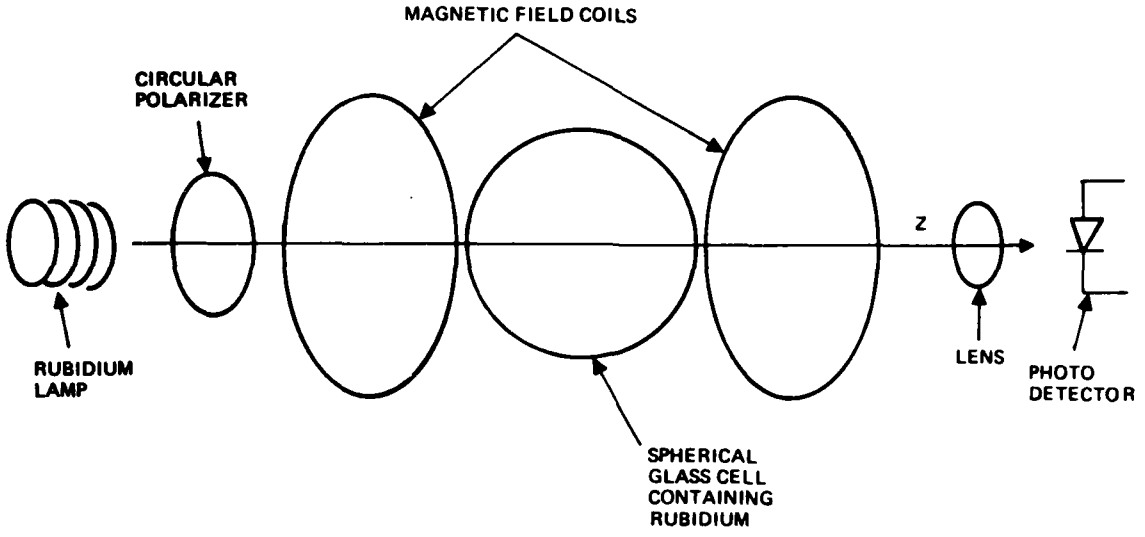

Figure 2-1. Arrangement of the System

The cell is maintained at a constant temperature in order to produce rubidium vapor of the required density. The light is the source of angular momentum, oriented along the direction of the light beam which, when absorbed by the rubidium, causes angular momentum to transfer to the rubidium atoms. This results in the rubidium atoms having a net angular momentum or spin polarization in the same direction as the light beam. The overall magnitude of the spin polarization is governed by an equilbrium between the rate of angular momentum absorption from the light (pumping process) and angular momentum losses via other interactions or relaxation processes. "Pumping" and "relaxation" both refer to angular momentum transfer processes, the distinction being whether there is a net gain or loss in the transfer.

One of the rubidium relaxation processes is the spin exchange interaction which results in some of the net angular momentum of the rubidium system being transferred to the noble gas nuclear

spin system. This results in the creation of a net angular momentum for the noble gas systems. The magnitude of the net noble gas angular momentum is governed by an equilibrium between the noble gas pumping and relaxation processes in a manner similar to that for rubidium.

First it is necessary to describe the optical pumping process in some detail from a quantum mechanical viewpoint. For the purpose of this discussion, the assumption is made that the alkali atom is described by a $^2S_{1/2}$ ground state with no nuclear spin. Therefore, the atoms are not influenced by any nuclear spin but possess only atomic spin. (This is not the actual case; but, for purposes of this discussion, it is an acceptable assumption.)

The energy level diagram of an alkali atom with a nuclear spin of zero in the presence of a magnetic field is shown in figure 2-2. The transition between the ground state and the first excited state ($^2S_{1/2}$ - $^2P_{1/2}$) is designated as D_1. The transition between the ground state and the second excited state ($^2S_{1/2}$ - $^2P_{3/2}$) is designated as D_2. $\pm m_j$ denotes the projection of electron spin angular momentum of the particular sublevel. n+ and n- are the population densities of the $m_j = +1/2$ and $m_j = -1/2$ ground state sublevels, respectively. The optical pumping cycle is composed of three stages:

a. Absorption of the pumping light by the ground state, or depopulation pumping

b. Excited state mixing and de-excitation or repopulation pumping

c. Ground state relaxation - including spin exchange processes

GUIDANCE & CONTROL SYSTEMS
5500 Canoga Avenue, Woodland Hills, California 91365

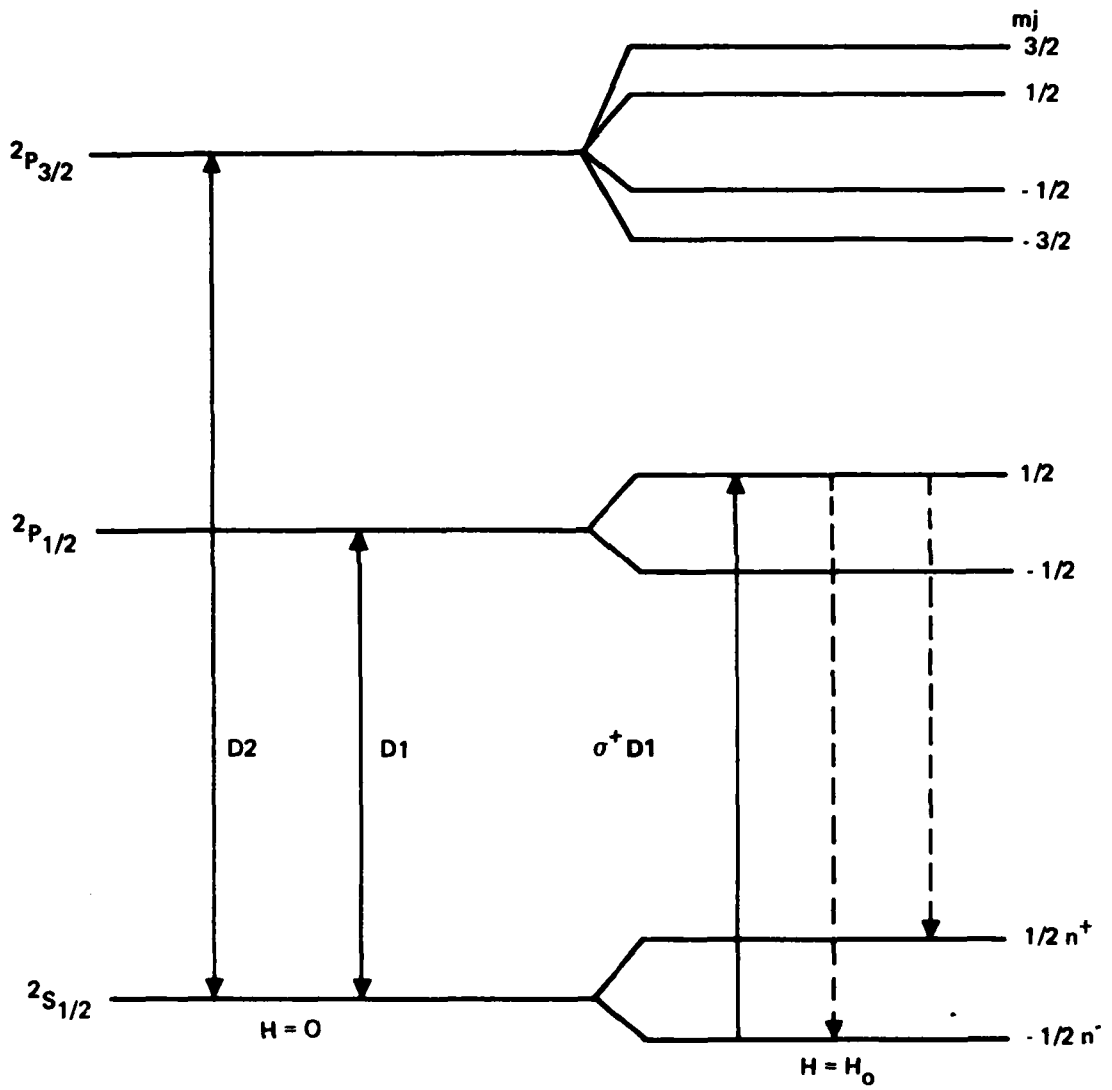

Figure 2-2. Energy levels are used to show excited states of the Rubidium atom

With an applied magnetic field of H_o, the atomic sublevels are split as shown in figure 2-2 at the horizontal point labeled $H = H_o$. The vapor is illuminated with circularly polarized, σ^+ D_1 light, propagating along the direction of the magnetic field, H_o. Using selection rules from quantum mechanics the absorption of the σ^+ light demands $\Delta m_j = +1$. With reference to figure 2-2, it is evident that for the σ^+ D_1 transition, only the atoms in the $m_j = -1/2$ ground state sublevel can absorb the light. This results in transitions to the $m_j = +1/2$ excited state sublevel. Assuming no mixing of levels in the excited state, any atom decaying from the excited state to the $m_j = +1/2$ ground state sublevel will tend to remain there, unable to absorb σ^+ photons. Although the excited state can decay to either of the ground state sublevels, those atoms returning to the $m_j = -1/2$ level are able to absorb another photon and reach the excited state again. The net effect of continued pumping of an assembly of atoms is to transfer the population of atoms from the -1/2 level to the +1/2 level. When this happens the rubidium vapor is said to be polarized by having transferred angular momentum from the light beam to the electronic states of the rubidium atoms.

For this study an atom is designated as either being polarized or unpolarized. Let the number of polarized atoms be S, where S is the density of atoms in the polarized state. For the case where all atoms are polarized, S = 1, or 100% polarization. An expression for S as a function of the spacial parameters is then needed.

The fundamental approach used describes the phenomenon inside the cell from a particle standpoint (Ref 2-4). The initial assumption is that at an elevated and constant temperature the rubidium atoms are uniformally distributed throughout the volume. The polarization at this time is random with the total ensemble polarization equal to zero From particle diffusion physics, the mass flow of the atoms is a vector and for an incremental volume as shown in figure 2-3, must equal zero.

GUIDANCE & CONTROL SYSTEMS
5500 Canoga Avenue, Woodland Hills, California 91365

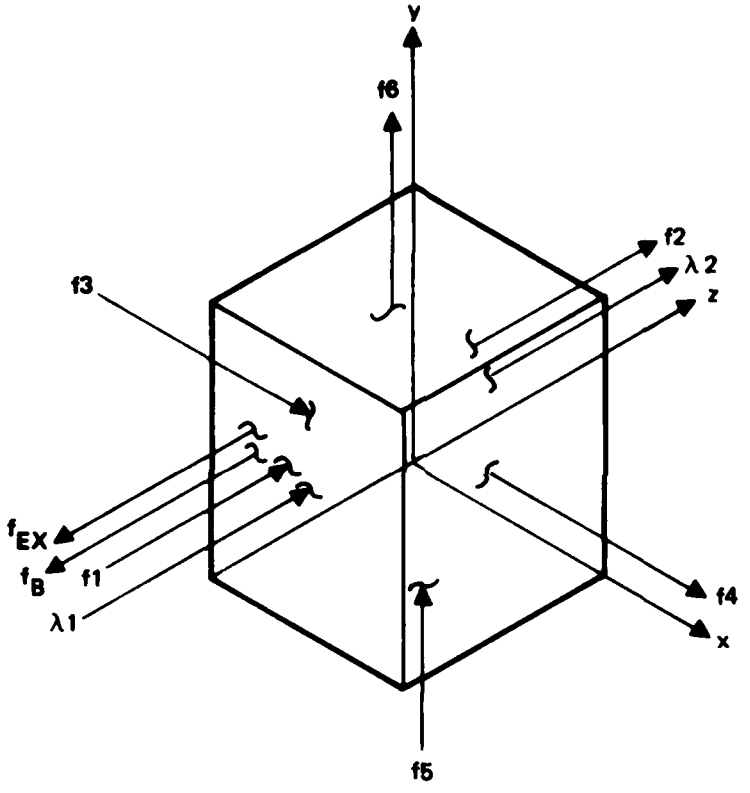

Figure 2-3. Incremental volume allows derivation of mathematical model

In Appendix A the detailed derivation of the system shown in figure 2-3 is carried out, and it is shown that the standard Laplace equation in three dimensions, or

$$\nabla^2 S = 0 \quad , \tag{2.1}$$

is obtained.

This describes the system in the steady state with no light being applied. When the cell is illuminated by the light beam, some of the atoms become polarized as described earlier. This then takes the form of an internal source of flux which in turn modifies equation (2.1) as

$$\nabla^2 S = -f_L \quad . \tag{2.2}$$

f_L is a function of the number of unpolarized atoms in the vapor and of the random process of light absorption. In this case

$$f_L = k_3 \Phi (1 - S) \tag{2.3}$$

where k_3 is the light absorption probability per atom per unit time and Φ is the light intensity in units of photons per cm^2 per sec.

When light first enters the cell the atoms at the front of the cell will absorb light first and become polarized. When the polarization in the remainder of the cell is zero this produces a gradient of polarization throughout the cell. The equation which governs this process is the diffusion equation. Equation (2.2) is modified to include this effect as

$$\frac{1}{D}\nabla^2 S = \frac{\partial s}{\partial t} - k_3 \Phi (1 - S) \tag{2.4}$$

where D is the diffustivity or diffusion constant. The effect of relaxation is considered next. The decay rates from the excited

state sublevels to the ground state sublevels have an effect on the equilibrium polarization of the rubidium. One such mechanism is the collisions of the alkali atoms in the $^2P_{1/2}$ state with the buffer gas atoms and the noble gas atoms in the cell. These collisions cause transitions between the sublevels in the excited state from $m_j = +1/2$ to $m_j = -1/2$, thereby changing the relative repopulation rates of the ground state sublevels. The mixing of the excited state sublevels is proportional to the density of the buffer gas atoms in the cell. The relaxation rates are measured for this system and are considered known constants. Relaxation is thought of as the opposite of pumping and for the model in figure 2-3 another mass flow term is added to account for this mechanism. This term is a function of the concentration of the polarized atoms and the rate at which they will relax.

This term is included in equation (2.2) as

$$f_R = -KS \tag{2.5}$$

There are three main types of collisions which induce transitions between the ground state sublevels:

a. Collisions of the alkali atoms with the foreign gas atoms in which spin exchange is not involved

b. Spin exchange collisions between the alkali atoms and the noble gas nuclei

c. Collisions of the atoms with the walls of the cell

In the simplest case, collisions with the buffer gas atoms induce transitions in each alkali ground state sublevel with equal

probability. Each level is driven to its equilibrium value for which another flow rate term is written as

$$f_B = -k_1 S \tag{2.6}$$

where k_1 is proportional to the foreign gas density. Spin exchange between the alkali atoms and the noble gas nuclei creates nuclear spin polarization and is a very important characteristic for the NMR gyro operation. This study, however, treats the polarization of the electronic spins of the rubidium. The polarization of the nuclear spin of the noble gases, related to the polarization of the alkali atoms, is not treated here. The spin exchange relaxation process as it applies to rubidium provides another relaxation or flow term

$$f_{ex} = -k_2 S \tag{2.7}$$

All of these flow rates are added to equation (2.2) as modifiers giving

$$\frac{1}{D}\nabla^2 S = \frac{\partial S}{\partial t} - k_3 \Phi(1 - S) + k_1 S + k_2 S \quad . \tag{2.8}$$

Under steady state conditions (8) becomes

$$\frac{1}{D}\nabla^2 S = - k_3 \Phi(1 - S) + k_1 S + k_2 S \quad . \tag{2.9}$$

The collisions of the alkali atoms with the walls of the cell are considered as boundary conditions for equations (2.8) and 2.9). However the walls of the cell do not always reduce the polarization to zero at the boundary. It has been observed (Ref. 2-5) that the rubidium atoms do not relax immediately, but tend to stick to the glass surface and retain their polarization. This case is modeled by allowing some finite value of polarization at the walls.

The polarization at the walls is not known. However, it is possible to find a relationship for the gradient of the polarization at the walls. The required boundary conditions can be produced by considering the walls as reflecting the flux partially or adsorbing the flux partially, depending on the wall surface. A probability of absorption R, is assigned to different wall coatings where $0 \leq R \leq 1$. The gradient is then written as

$$\frac{\partial S}{\partial z} = Rf_i \qquad (2.10)$$

where f_i is the flux entering a small incremental volume adjacent to the wall. We can write the f_i term as the polarization at the wall times the mean velocity, $\bar{v}_{rel}$, giving

$$\frac{\partial S}{\partial z} = R\bar{v}_{rel}S \quad . \qquad (2.11)$$

Under this boundary condition, when R = 0 the gradient is equal to zero and the walls will reflect all polarization. For the opposite case where R = 1 the gradient at the walls is equal to $\bar{v}_{rel}S$. With S a positive number less than 1 and taking into account that $\bar{v}_{rel}$ is a large number, this corresponds to a completely depolarizing wall with the polarization at the wall equal to zero.

The parameters of equation (2.9) are defined in the following manner. D is the coefficient of diffusion for the rubidium atoms in the presence of the buffer gas. The pressure dependence of D has the form

$$D = D_o \frac{P_o}{P} \qquad (2.12)$$

where P_o is standard atmospheric pressure, P is the actual partial pressure of the buffer gas pressure and D_o is the diffusion coefficient at standard conditions.

The k terms of equations (2.6) and (2.7) are formulated as

$$k = N_o \sigma \bar{v}_{rel} \frac{P}{P_o} \tag{2.13}$$

where N_o is the density of the gas atoms at atmospheric pressure. The actual density, N at pressure P is

$$N = N_o \frac{P}{P_o} \quad . \tag{2.14}$$

σ is the appropriate cross section which characterizes rubidium gas collision, and $\bar{v}_{rel}$ is the mean relative velocity of the rubidium and the gas atoms. This formulation allows simulation of relaxation characteristics due to the buffer gas provided that the cross section for the interaction has been measured.

The coefficient k_3 in equation (2.3) is related to the incoming light in the following way

$$\Phi k_3 = \int_0^\infty I_\upsilon \sigma_\upsilon d_\upsilon \tag{2.15}$$

where I_υ is the spectral density distribution of the incident light in the photons per cm^2 per second per unit frequency υ, and σ_υ is the cross section for absorbtion of a photon of the frequency υ. The light intensity does not remain constant throughout the cell, but is reduced in magnitude by the absorption by the rubidium. For this study it is assumed that the spectral distribution does not change through the cell but is constant. A partial differential equation for the variations in light intensity, Φ, across the cell, taking into account the polarization of the rubidium, as derived in Appendix A is

$$\frac{\partial \Phi}{\partial z} = k_3 N_{Rb} \Phi (1 - S) \tag{2.16}$$

where N_{Rb} is the rubidium number density. The boundary condition for this equation is established by the uniform input light intensity from the lamp, which gives at the front surface of the cell

$$\Phi = \Phi_o \quad . \tag{2.17}$$

The light intensity after it leaves the cell is not known because the absorption of the light depends on the polarization in the cell.

For discussions of gyro operation, the direction of the light is chosen as the direction z of a cartesian coordinate system. This has been done historically in optical pumping experiments. For gyro operation the polarization along the three principle directions, X, Y, and Z, of the applied magnetic fields is of interest. This study and simulation also uses the cartesian coordinate system. The shape of the cell determines the boundary locations of the problem. The spherical and cylindrical boundaries are easily expressed in terms of a rectangular coordinate system. The input light is applied only in one direction. Depending on the shape of the cell different absorption characteristics of the light can result.

Certain assumptions were made in arriving at the preceding model. This model was obtained from a particle standpoint instead of from a quantum mechanical point of view. However the results of quantum mechanics were used to obtain some of the parameters, such as the probability of an atom being pumped. Various cross sections are given as parameters in this study without deriving expressions for each mechanism from basic principles. These parameters are the result of laboratory experiments. It is also assumed that the light is well columnated and has little dispersion. This condition is nearly realized experimentally if a lens system is used between the lamp and the cell, which is the usual case.

For this problem it is shown that to calculate the spacial distribution of polarization of optically pumped rubidium inside a glass cell it is necessary to solve two simultaneous coupled partial differential equations. A solution of these equations is possible using a digital computer employing an implicit technique which requires many iterative cycles to obtain a solution. With modern digital computers such as the DEC VAX 780, this is not a great challenge nor is it very time consuming. The details of the approach to the computer simulation used in this study are presented in Appendix B.

The result of the simulation is a plot of the polarization distribution in the steady state inside the cell.

For the transient case, which is often encountered in experimental work, the simulation is more difficult. To obtain meaningful results in both time and space involves performing a steady state solution at each time interval. The potential for instability increases along with many more iterative cycles required to obtain the solution. The transient case was not considered in detail at this time.

A computer program has been written to solve these coupled partial differential equations in one dimension. This program was used to produce the results of this report.

2.3 RESULTS

The first version of the rubidium polarization distribution model is shown schematically in figure 2-4. This version, corresponding to a cylinder of infinite radius, has perfectly circularly polarized incident light impinging on a cell of length L. The faces (walls) may range from perfectly depolarizing to perfectly non-depolarizing. The program, as written, allows for input parameters of the incident light intensity, the wall depolarization parameter, the cell length, the temperature, and finally the gas fill pressures for xenon, helium, and nitrogen.

GUIDANCE & CONTROL SYSTEMS
5500 Canoga Avenue, Woodland Hills, California 91365

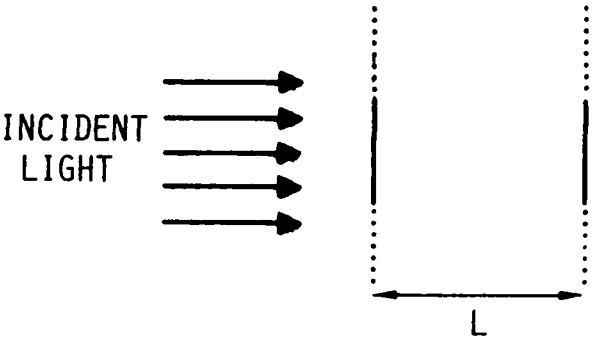

Figure 2-4. Schematic Representation of One Dimensional Rubidium Polarization Model

Several examples of input parameters have been selected to illustrate the results of the modeling.

Figure 2-5 displays the effect of light intensity on the rubidium polarization across a sample cell. Here all parameters except light intensity were held constant. Notice that at high light intensity for a cell of length 1.3 cm there is little or no rubidium polarization gradient except at the cell boundary. The case presented here is for perfectly depolarizing walls. As the major rubidium field gradient effect, other than that due to the wall, occurs at low light intensity, the rest of the simulations were carried out for such an intensity. In fact, in the experimental apparatus the light intensity is rather high. It should be noted that all these calculations predict an unusually high rubidium polarization. That results from the assumption of perfectly polarized incident light and the neglect, in this first version of the modeling, of any effect due to spectral profile of the pumping light. However, it is not expected that the essential form of the results presented here will be substantially altered in the later versions.

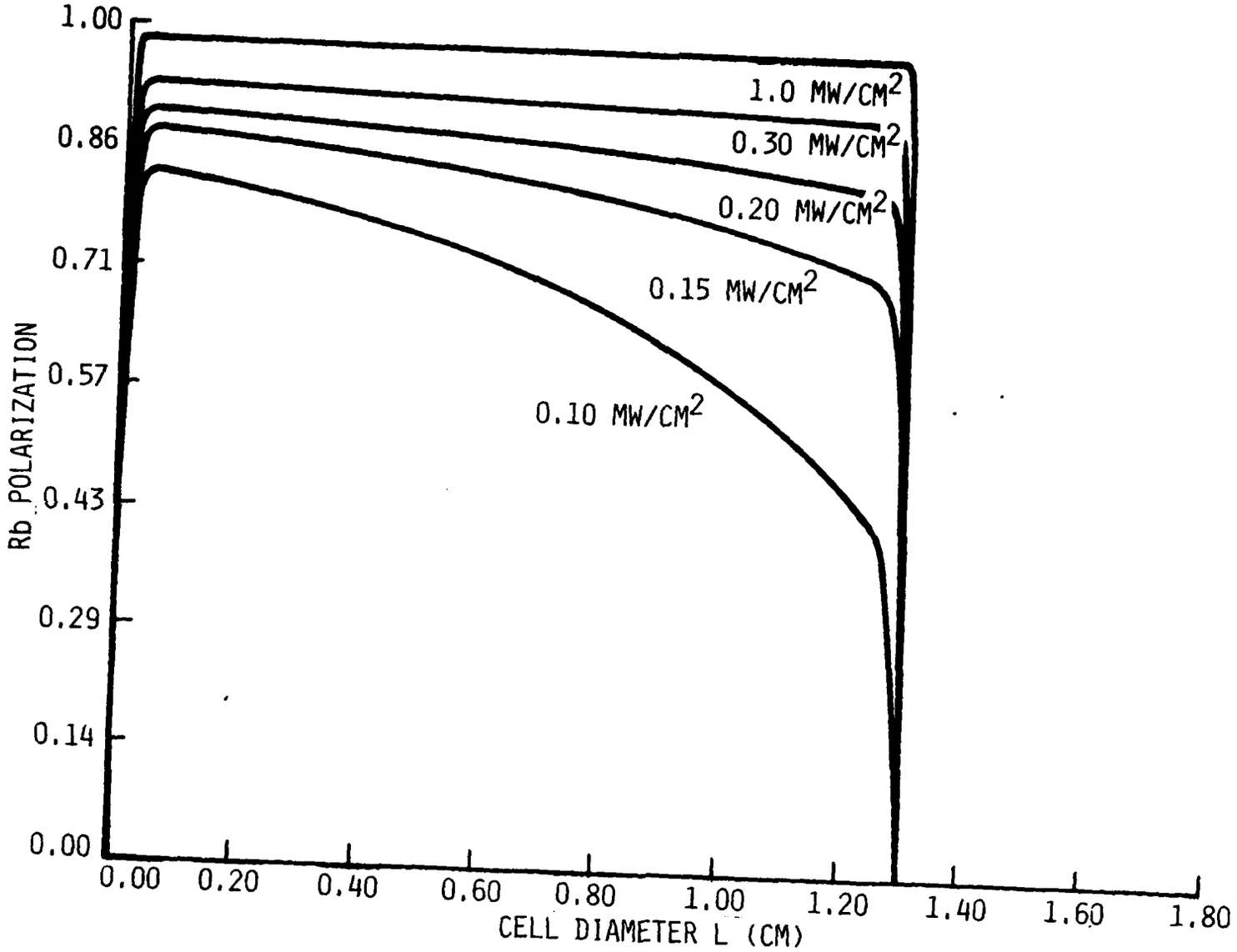

Figure 2-5. Effect of Light Intensity on Rubidium Polarization

Figure 2-6 shows the effect of the wall on the rubidium polarization distribution for a case when all other parameters are held constant. Note that the major differences occur at the wall although there is a small effect within the cell body. The slightly lower polarization for perfectly depolarizing walls is due to the fact that more of the light intensity is absorbed in the region of the cell near the light source, and less pumping light arrives at the region farther from the light source.

Figure 2-7 shows the effect of cell size. Here parameters were chosen corresponding to figure 2-6 for the perfectly non-depolarizing wall. The results show, for these parameters, that the rubidium polarization drops off about 50% across a cell of length 1.3 cm and close to 100% at a length of 2 cm. Thus cell size could become very important in the event that, as illustrated here, the light intensity is very low. Calculations of this type aid in determining minimum required light intensity for cells of various sizes.

Figure 2-8 illustrates the effect of temperature on rubidium polarization. For this case, all parameters except temperature were held constant and the same low light intensity as for figures 2-6 and 2-7 was chosen. The effect shown here illustrates that at higher temperatures the rubidium vapor becomes so dense that more of the light is absorbed causing a very large effect at 100C. In gyro operations there are also considerations such as rubidium magnetometer sensitivity and gyro bias temperature sensitivity, and it is found practical to operate close to 80C with high light intensity.

GUIDANCE & CONTROL SYSTEMS
5500 Canoga Avenue, Woodland Hills, California 91365

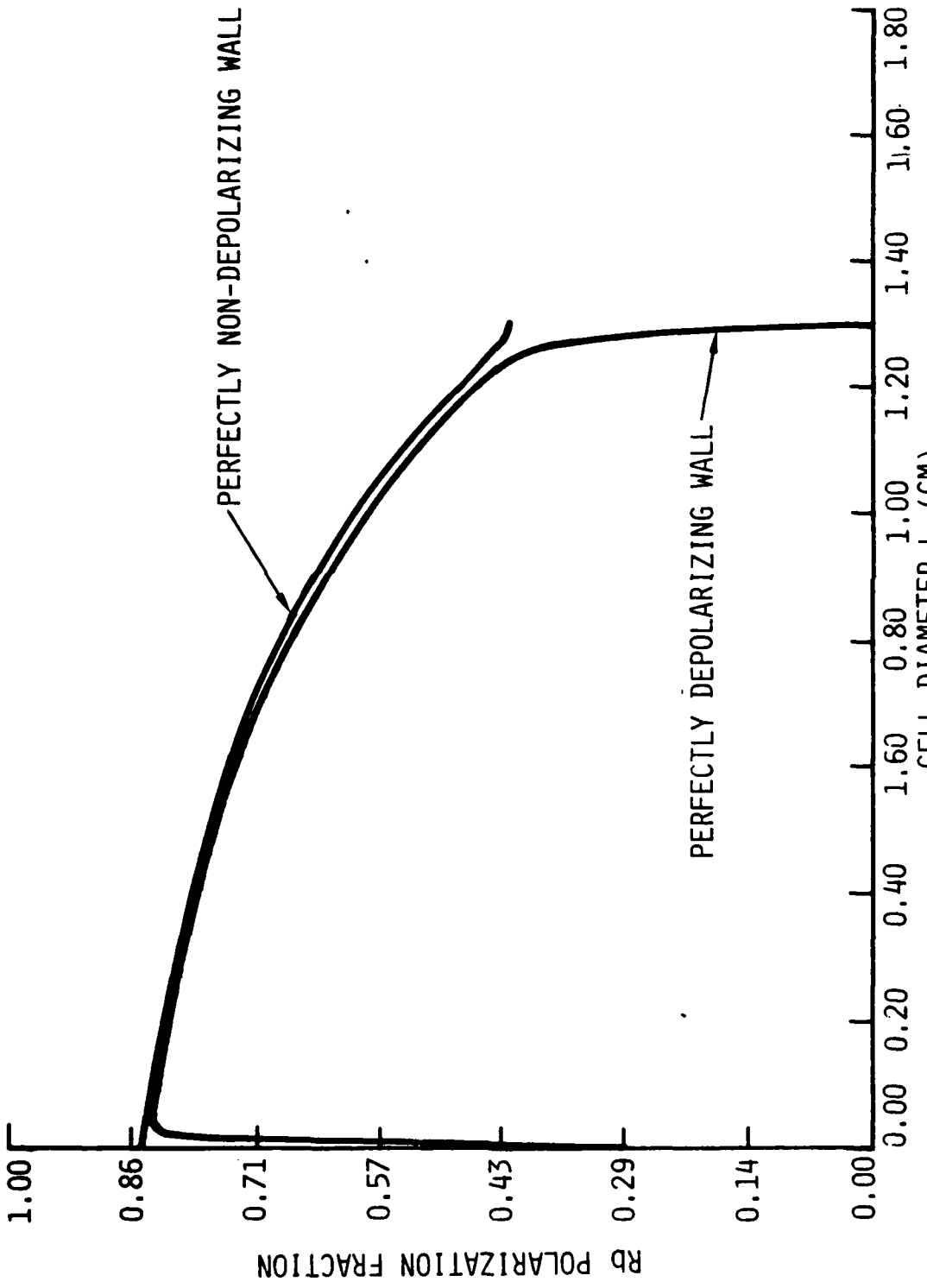

Figure 2-6. Rubidium Polarization Wall Effect

GUIDANCE & CONTROL SYSTEMS
8800 Canoga Avenue, Woodland Hills, California 91365

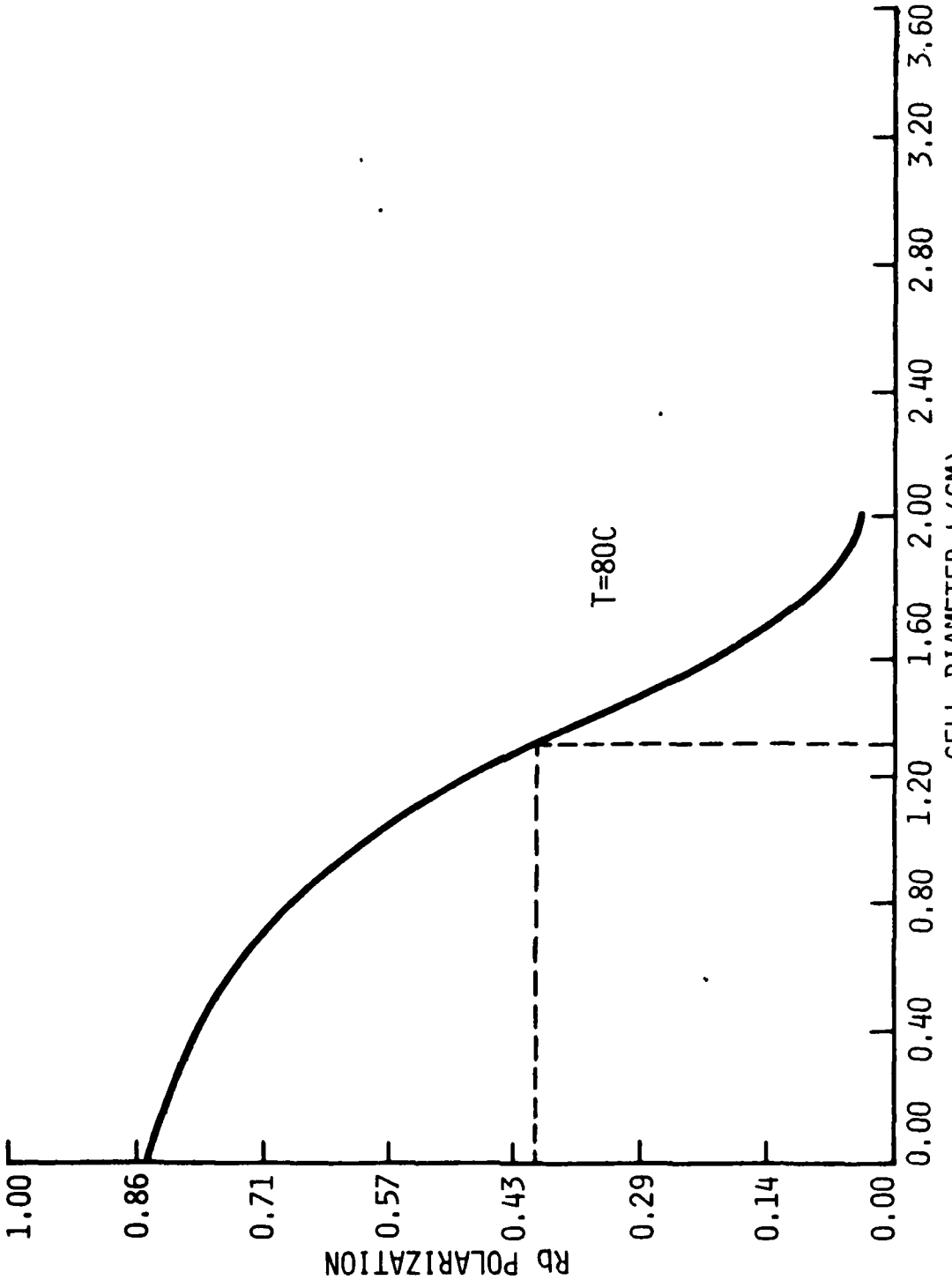

Figure 2-7. Effect of Cell Size

GUIDANCE & CONTROL SYSTEMS
5500 Canoga Avenue, Woodland Hills, California 91365

FSCM 06481

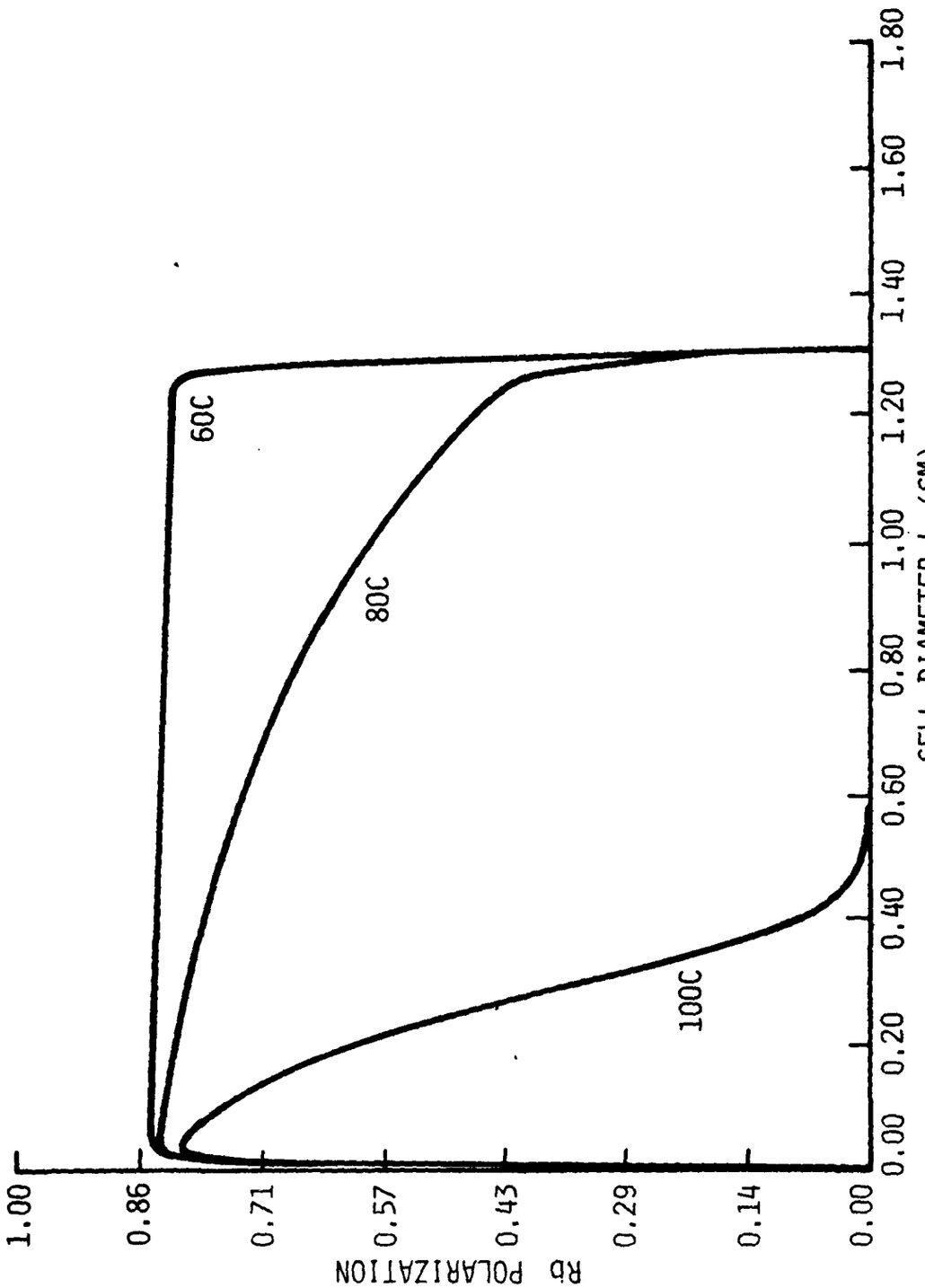

Figure 2-8. Effect of Temperature on Rubidium Polarization

Finally, figure 2-9 illustrates the effect of a buffer gas pressure. The three traces in figure 2-9 represent three different helium pressures while all other parameters are held constant. Again, the same low light intensity was chosen in order to illustrate better the effect due to pressure. This figure illustrates very well why a buffer gas is added to optically pumped systems. The higher the buffer gas pressure the closer the polarized species may approach to the wall without being depolarized by the relaxing effect of the wall. For lower buffer pressure, the wall effect is more noticeable.

The results presented here are well illustrated by experimental results presented previously (Ref 2-2). This report presents selected new experiments which illustrate certain effects shown in figures 2-5 through 2-9.

It is well known in NMR experiments that a static field inhomogeneity along the direction of the D.C. magnetic field will be a source of transverse nuclear relaxation. In order to illustrate effects due to rubidium field gradient two types of experiments are carried out. One has the magnetic field (precession field) perpendicular to the direction of the light axis. In that case, in the idealized model, the rubidium field gradient is perpendicular to the main field and does not contribute strongly to the transverse relaxation time. In the second type of experiment the magnetic field (precessicn field) is along the light beam direction and any inhomogeneity due to rubidium polarization will be felt. As discussed previously, (Ref 2-2) in the event that an external as well as an internal field gradient exists, two different transverse relaxation times would be expected in the second type of experiment depending on whether σ^+ or σ^- circularly polarized light were used.

GUIDANCE & CONTROL SYSTEMS
5500 Canoga Avenue, Woodland Hills, California 91365

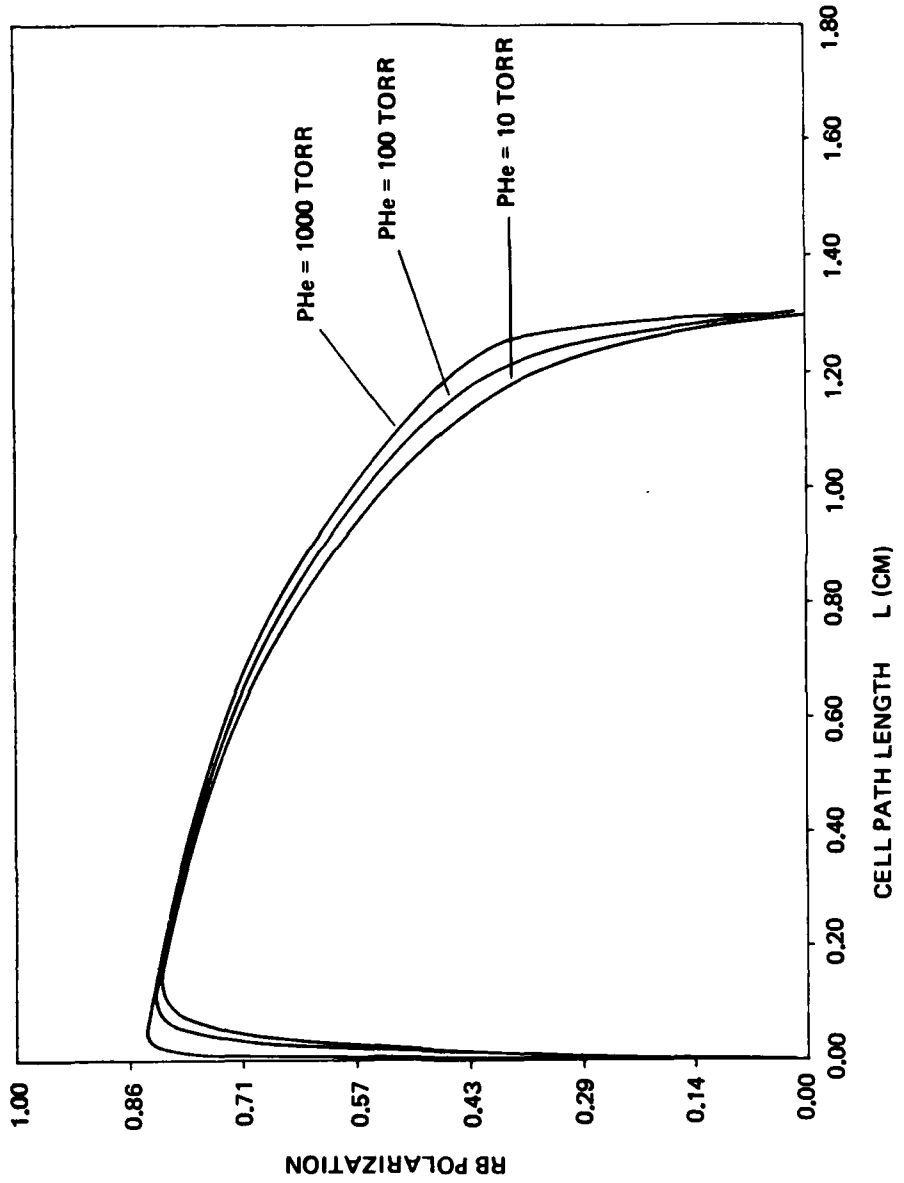

Figure 2-9. Effect of Pressure on Rubidium Polarization

In the event that there is either no external field gradient arising from inhomogeneities in the precision field directed along the light beam or that there is no internal field arising from a rubidium polarization gradient, it is expected that the observed transverse relaxation times would be the same if either σ^+ or σ^- circularly polarized pumping light is used.

In table 2-I a few transverse relaxation time data are presented for the two types of experiments. The circular polarizers are labeled "A" and "B". In the experiment where the precession field is perpendicular to the light beam the relaxation time is found to be the same in both polarizations and only results for polarizer "A" are presented. The marked difference between the relaxation times in that experiment and in the experiment with the field parallel to the light beam demonstrates the existence of a field gradient in the case where the field is parallel to the light axis. The small, but very real, differences in the relaxation times for the two light polarizations in that experiment illustrate the existence of both an external and an internal field gradient in that system. The differences in relaxation times found in the two types of experiments simply illustrate that some field gradient effect exists for the field parallel experiment but does not distinguish as to whether an internal gradient is present. The example presented in table 2-I was selected to illustrate the internal field gradient effects. In fact it is found for a number of systems of small cells irradiated with high light intensity that there is no difference in relaxation times for the two experiments and no dependence on choice of polarization. Ths is a very important result as far as gyro operation is concerned.

TABLE 2-I. EXAMPLE OF EFFECT OF RUBIDIUM POLARIZATION DISTRIBUTION ON TRANSVERSE RELAXATION TIMES

	T_2(Sec) at 100C	T_2(Sec) at 80C
Field parallel to Light Beam		
Polarizer A	48	134
Polarizer B	45	126
Field perpendicular to Light Beam		
Polarizer A	77	210

2.4 CONSIDERATIONS FOR FUTURE WORK

The modeling presented here is being extended to include more general cell shapes. Combined with experiment, the modeling will be used to optimize pumping light intensity for various cell sizes and fills.

2.5 REFERENCES

2-1. S. Legowski, Bull. de L'Academie Polonaise des Sciences, 14, 525 (1968).

2-2. A. T. Nicol, U.S. Air Force Office of Scientific Research Final Technical Report, Contract No. F49620-77-C-0047, 1982 (unpublished).

2-3. W. Happer, Rev. Mod. Phys. 44, 169 (1972).

2-4. W. J. Karplus and V. Vemuri, Digital Computer Treatment of Partial Differential Equations, Prentice-Hall Inc., Englewood Cliffs, N.J., 1981.

2-5. G. W. Series, Contemp. Phys. 2, 487 (1981).

Litton GUIDANCE & CONTROL SYSTEMS
5500 Canoga Avenue, Woodland Hills, California 91365

FSCM 06481

SECTION III

THE IMPORTANCE OF DIRECT DIPOLE-DIPOLE SURFACE RELAXATION OF ^{129}Xe IN SMALL SAMPLE CELLS

3.1 INTRODUCTION

In recent years the gas phase nuclear polarization and relaxation of the spin 1/2 isotope of xenon, ^{129}Xe, has been the subject of several studies (Ref 3-1 to 3-3). Among the reasons for interest in this system are applications in a nuclear magnetic gyro (Ref 3-4) preparation of polarized nuclear targets, and, more recently, the possible improvement in the fusion process by use of polarized nuclei (Ref 3-5). While previous studies of ^{129}Xe have been confined to systems in which the sample cells were relatively large (Ref 3-1 to 3-3) (15 ml), this section presents results for the first in a series of studies of small (1 ml) sample cells where surface effects become important for ^{129}Xe. In the system under investigation the xenon nuclear polarizaion is achieved through a spin exchange process in an optically pumped rubidium-xenon system. In order to probe for possible surface relaxation of ^{129}Xe due to the direct dipole-dipole interaction, cells coated with either RbH or RbD have been investigated. This is an experiment analogous to that of Bouchiat and Brossel (Ref 3-6) who investigated rubidium relaxation on ordinary paraffin and deuterated paraffin cell surfaces. However their concern was with the alkali. This study examines, for the first time, the relative efficiency of hydrided or deuterided surfaces for relaxation of nuclear polarization of a noble gas.

There are various mechanisms known to govern nuclear relaxation of spin 1/2 noble gases on surfaces. Fitzsimmons, Tankersly, and Walters (Ref 3-7), considering the case of ^{3}He relaxation in cells prepared from quartz, pyrex, and two aluminumosilicate glasses, discussed two surface relaxation mechanisms. One was a permeation

controlled relaxation due to the diffusion of helium into and back out of the cell wall material. The other, applicable to our case, was an adsorption controlled mechanism. As will be seen, the study reported here differs from others in that it involves a system where surface energies and sticking times are expected to be the same, while local fields experienced by the nuclear species will differ. In Section IV experiments on surfaces of several different types providing both different surface energies and different apparent local fields, will be discussed. The results presented in this report suggest that, for ^{129}Xe surface relaxation in cells buffered sufficiently to inhibit the wall interactions of the alkali but not of the noble gas isotopes, differences in magnitude of local nuclear magnetic fields at the surface do not control the relaxation process.

3.2 THEORETICAL BACKGROUND

Previous studies of surface relaxation of spin 1/2 noble gases have been confined to the study of the other spin 1/2 isotope, ^{3}He (Ref 3-7, 3-8). In the ^{3}He case there are two mechanisms for surface relaxation, a permeation controlled relaxation and a surface adsorption controlled relaxation. The latter is the appropriate model for ^{129}Xe, an isotope not susceptible to the same degree of diffusion into glass as helium.

Most generally, the expression for T_1, the longitudinal relaxation time of the spin 1/2 system on the surface, is expressed as (Ref 3-7)

$$T_1 = \frac{N}{n}\left(t_s + T_s\right) \quad , \tag{3.1}$$

where t_s is the average wall collision sticking time (or dwell time), T_s is the characteristic relaxation time for the species (^{129}Xe) on the surfaces, N is the number in volume V of atoms of the species under consideration, and n is the number of these

GUIDANCE & CONTROL SYSTEMS
Litton 5500 Canoga Avenue, Woodland Hills, California 91365

atoms interacting with the surface at any instant. This expression is general for surface relaxation as long as n<<N. The expression does not depend on the specific surface relaxation mechanism proposed. It has been shown (Ref 3-7) that expression (3.1) takes the form

$$T_{1A} = \frac{2\ V\ e^{-2E/kT}}{A\ \bar{v}\ (\gamma \bar{H}_1 t_s^o)^2} \quad . \qquad (3.2)$$

In equation (3.2) V is the volume of the cell, A is the effective surface area which need not be equal to the apparent geometrical area, E is the surface adsorption energy, $\bar{v}$ is the mean thermal velocity of the atomic species (^{129}Xe), $\bar{H}_1$ is an average local magnetic field at the surface site, t_s^o is the sticking time in the high temperature limit, and T is temperature in Kelvins. The physical constants k and γ are specified. Assumptions made in obtaining equation (3.2) were that $\gamma \bar{H}_1 t_s << 1$ and

$$T_s = \frac{t_s}{2(\gamma \bar{H}_1 t_s)^2} >> t_s$$

These can be shown to be reasonable for cases where t_s is sufficiently short, E is low enough and $\bar{H}_1$ is due to nuclear species. For helium E ~ .01 - .1 ev and $t_s \leq 10^{-12}$ sec at temperatures of interest (Ref 3-7). The sticking time is described by $t_s = t_s^o\ e^{+\ E/kT}$ where t_s^o is the high temperature sticking time expected to be on the order of a molecular vibration time (~ 10^{-12} sec). Assuming a local field arising from nuclei in atoms on the surface to be on the order of 1 gauss (Ref 3-9) and using the value of $-7.4 \times 10^{+3}$ rad/sec gauss, the gyromagnetic ratio for ^{129}Xe, the conditions for equation (3.2) are readily fulfilled. The assumptions could break down at the extreme where E = 0.3 ev (observed for xenon on platinum (Ref 3-10) and the local field is due to an unpaired electron spin (paramagnetic center). For the systems under discussion in this paper the assumptions are

probably valid. The RbD or RbH coating effectively shields the ^{129}Xe from paramagnetic centers. There is however, another consideration.

In the event that there is more than one surface site, i, of different adsorption energy E_i, and assuming no correlation between relaxation on the various sites then equation (3.2) becomes

$$T_{1A} = \frac{2\,V}{A\,\bar{v}\,\gamma^2 t_s^{o\,2}} \left(\sum_i \frac{1}{\bar{H}_{1_i}^2}\, e^{-2E_i/kT} \right) \qquad (3.3)$$

In their study of helium adsorbed to aluminosilicate glass Fitzsimmon, et al, found evidence for two different adsorption sites (Ref 3-7). For cells studied here, for example, there is rubidium metal present which may or may not be covered with hydride or deuteride.

The question of the expected magnitude of the adsorption energy of xenon on surfaces requires thorough consideration not only because it can affect the validity of equations (3.2) and (3.3) but also because it is of interest for interpreting results of experiments where (3.2) and (3.3) cannot represent the proper model (e.g., a quadrupolar nucleus such as ^{131}Xe) but the surface binding energy (and sticking time) is still important for the model in question. Fitzsimmons, et all (Ref 3-7) found for He a surface adsorption energy of .01 ev on pyrex and .01 ev and .1 ev on aluminosilicates although they could have fit their data to a range of values. One would speculate, for example, that the binding energy for helium on a silica site might be different from that of helium on an alumina site. In any event, recent results for Ar and Xe adsorbed on alumina suggest a larger adsorption energy for those species (Ref 3-11, 3-12) than for helium, and a slightly larger adsorption energy for Xe on pyrex has been reportd in ^{131}Xe studies (Ref 3-13, 3-14). An adsorption energy of .5 ev was predicted for Ar

GUIDANCE & CONTROL SYSTEMS
Litton 5500 Canoga Avenue, Woodland Hills, California 91365

FSCM 06481

on Al_2O_3 with the atom a distance of 2.9 A from the surface in good agreement with the experimental result of 0.3-0.4 ev for that system. Similar results are cited for the Xe-Al_2O_3 system, but numbers are not given. In view of the known larger polarizability of xenon and despite its larger Van der Waals radius it is easy to believe that the effect for xenon could be even larger. If that is the case, the assumptions leading to equations (3.2) and (3.3) would still be valid as long as the magnetic site on the surface is not due to an unpaired electron spin. One way to try to sort out contributions of various different effects is to consider a system in which Ea and T_s are held constant while $\bar{H}_1$ is varied. Such a system is the subject of this paper.

In the event that sticking times and adsorption energies are the same for different samples then it is known that the relaxation rate of a nuclear spin I interacting with a second nuclear spin I', if dominated by the direct dipole-dipole interaction, is a simple proportionality.

$$\left(\frac{1}{T_2}\right)_I \propto \frac{\gamma_I^2 \gamma_{I'}^2}{r_{II'}^6} I'(I'+1) \qquad (3.4)$$

where $(1/T_2)_I$ is the transverse relaxation rate of spin I, γ_I is the gyromagnetic ratio for spin I. $\gamma_{I'}$ is the gyromagnetic ratio for spin I', I' is the spin of spin I' (1/2 for ^1H, 1 for ^2H) and $r_{II'}$ is the distance between I and I'. As the deuteron has spin 1 and a gyromagnetic ratio of 4107 radian sec^{-1} $gauss^{-1}$ while the proton has spin 1/2 and a gyromagnetic ratio of 26753 radian sec^{-1} $gauss^{-1}$, one would predict a factor of 16 increase in relaxation time for ^{129}Xe relaxing on RbD over that found on RbH if its relaxation is dominated by the direct dipole-dipole surface interaction.

GUIDANCE & CONTROL SYSTEMS
Litton 5500 Canoga Avenue, Woodland Hills, California 91365

Any significant contribution to the direct dipolar relaxation of ^{129}Xe by the surface cation, Rb^+, (spin 3/2, gyromagnetic ratio 8750 rad sec^{-1} $gauss^{-1}$) can be ruled out by the $1/r_{II}^6$' factor on the basis of possible distance of closest approach of the two nuclei. Thus, if the ^{129}Xe is significantly affected by the direct dipolar interaction on the surface, a definite difference in ^{129}Xe relaxation times would be expected in comparing hydride and deuteride cells. This is to be expected even though the deuterium gas used in cell preparation contained significant hydrogen which reduces the factor of 16 to about 4. Practically speaking, this means that if a T_2 for ^{129}Xe of 80 sec is observed (a typical value in DMG cells at 80C) in a rubidium hydride coated cell then a T_2 of 320 sec should be observed in a rubidium deuteride coated cell if the relaxation is completely dominated by direct dipolar surface interaction.

As is well known, however, an important source of ^{129}Xe relaxation in these NMR cells is that due to gas phase interaction with rubidium (Ref 3-2). An expression for the total relaxation of the spin system can be written as

$$\frac{1}{T_2} = N_{Rb}\sigma\,\bar{v} + \frac{1}{T_2'} \qquad (3.5)$$

where the first term on the right hand side of equation (3.5) represents the gas phase relaxation rate. N_{Rb} is the rubidium density, σ is the exchange cross section and $\bar{v}$ is the relative Rb-Xe velocity. All other relaxation rates are incorporated into $1/T_2'$. Those other relaxation rates include effects due to any field inhomogeneity and effects due to wall interactions. For the experimental setup and cell types used in the experiments reported here it has been demonstrated that field gradients are

insignificant, (Ref 3-15) and hence $1/T_1'$ may be viewed as an effective wall rate. Thus equations (3.5, 3.4 and 3.3) provide

$$\frac{1}{T_2} = N_{Rb}\sigma\bar{v} + C\Sigma_i \frac{\gamma_{S_i}^2 I_i' (I_i' + 1)}{r_{II}^6} e^{2E_i/kT} + \frac{1}{T_2''} \qquad (3.6)$$

In this expression the first term on the right side has already been discussed. In the second term C is a constant. I_i' represents the spin that I (^{129}Xe) is interacting with in a direct dipolar interaction in which the atom containing nucleus I is adsorped to a site i close to I_i' with binding energy E_i. Any non-dipole-dipole wall relaxation mechanism rates are denoted by $1/T_2''$. Over the temperature range of interest all terms except the first are only very weakly temperature dependent with the major source of temperature dependence of the first term due to the rubidium vapor density. It has therefore become customary in these experiments to plot $1/T_2$ versus N_{Rb}. The resulting plot gives the effective spin exchange times relative velocity as slope and wall rate as intercept. In the event that for two different samples the wall adsorption energies are the same and any effect given by $1/T_2''$ is the same, the calculated wall rates would be expected to reflect differences in local fields. In such a case equation (3.6) reduces to

$$\frac{1}{T_2} = N\sigma\bar{v} + C_1 \Sigma_i \frac{\gamma_{S_i}^2 I_i' (I_i' + 1)}{r_{II}^6} + C_2 \qquad (3.7)$$

where C_1 and C_2 are constants which are the same for both types of cells. To the extent that the direct dipolar interaction is an important source of wall relaxation, differences in wall rates for the two types of cells are expected.

3.3 EXPERIMENT

3.3.1 Cell Preparation and Analysis

Twelve 1 ml pyrex cells were prepared containing ample ^{87}Rb, 0.5 torr ^{129}Xe, 2.5 torr ^{131}Xe, 100 torr He, 40 torr N_2, and 10 torr of either D_2 or H_2. (1 torr of gas corresponds to a number density of 3.54×10^{16} molecules/cm^3). The rubidium metal content was monitored with differential scanning calorimetry (DSC) by making use of the known heat of fusion at the melting transition which, at 39C, is in a convenient range for this determination. Through careful calibration, using especially prepared sample cells which were subsequently destructively tested for total rubidium content, it was possible to ascertain the Rb content of the NMR hydride and deuteride cells non destructively. The Rb metal content for these cells was found to range from 73 to 213 μ grams after sufficient time had elapsed for the hydrogen or deuterium to have reacted with the rubidium. Thus, the rubidium metal measured represents the unreacted portion of the total rubidium in the sample. After the NMR research progressed, selected cells were sent for independent destructive testing of the gas fill by means of mass spectroscopy.

3.3.2 NMR Studies

The cells, 6 containing D_2 and 6 containing H_2, were screened for NMR characteristics when first prepared. At that time Rb metal was distributed as a hemisphere inside the cells. Subsequent to the DSC studies the Rb was driven into the tip-off region by means of an oven running at 100C but having a cooled region close to the

cell tip. This "Rubidium Rearrangement Oven" is schematically illustrated in figure 3-1. The device includes cold fingers suitable for driving rubidium to the base for convenience in DSC experiments or to the tip for use in NMR experiments.

After driving rubidium to the cell tips, a series of NMR experiments were carried using an apparatus and methods which have been described previously (Ref 3-2). Temperature dependent studies were carried out in order to fit results to the terms of equation (3.5). This was followed by an aging study of cell properties at 80C which included some studies of the rubidium optical pumping characteristics (Ref 3-16) (rubidium magnetometer sensitivity and line width) in addition to noble gas polarization and relaxation characteristics. Aging was carried out at 80C over a period of about two months. This part of the experiment was aimed at determining the time necessary for attaining stable NMR parameters for both xenon isotopes. It had been observed that initial aging is necessary to bring the cells to a certain level of performance, but the actual aging characteristics were not known.

3.4 RESULTS AND DISCUSSION

As pointed out in the theoretical section there are well developed models for relaxation of a spin 1/2 system on interaction with a surface. In the model presented, ^{129}Xe should be much more affected by local fields than ^{131}Xe which has a factor of three lower gyromagnetic ratio than ^{129}Xe. In fact ^{131}Xe has a quadrupolar nucleus of spin 3/2 and is known to relax by an entirely different mechanism (Ref 3-13, 3-17). The ^{131}Xe relaxation is expected to depend on the strength of the quadrupolar interaction rather than the strength of a magnetic interaction such as the direct dipolar interaction. To the extent that this is true it is expected that there should be no difference between ^{131}Xe relaxation for deuteride versus hydride cells. It is expected that RbD and RbH will present very nearly the same surface binding energies,

Litton GUIDANCE & CONTROL SYSTEMS
5500 Canoga Avenue, Woodland Hills, California 91365

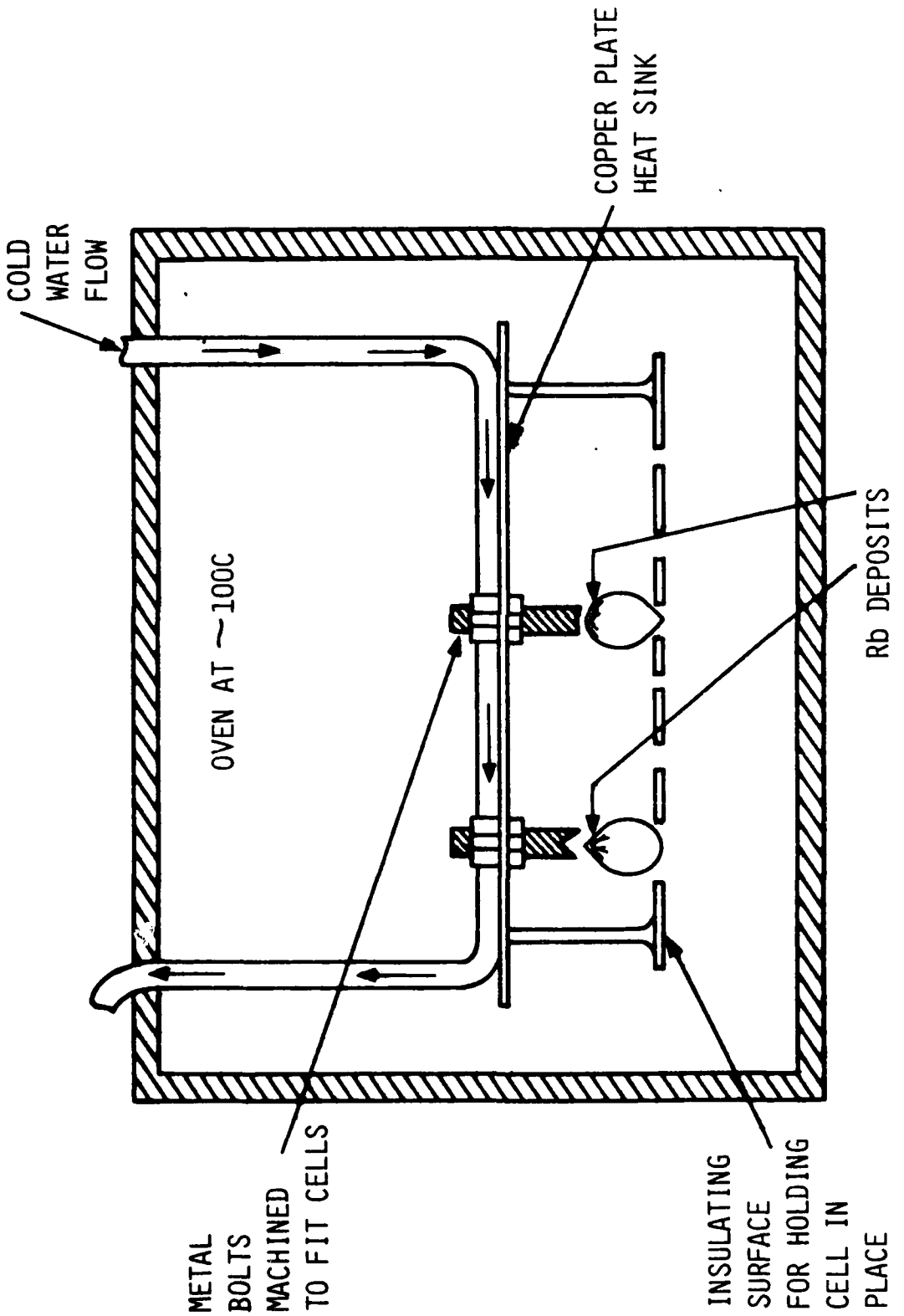

Figure 3-1. Schematic Representation of Rubidium Rearrangement Oven

dwell times and effective deformation of the electron cloud around the xenon nucleus. Thus reasonable models predict no difference for ^{131}Xe relaxing on these surfaces, but do predict differences for ^{129}Xe.

Figure 3-2 shows the results of an aging study at 80C in which the transverse relaxation times of the two species were monitored. The cells were aged at 80°C in an aging oven and periodically removed and studied. Data displayed for the first five weeks are averages for the six hydride and the six deuteride cells. Lines are drawn through the data points to aid the eye. At the end of the aging period one deuteride and one hydride cell were selected for destructive testing of gas fill by mass spectroscopy. Selected remaining cells were subjected to large (3-4 atm) external helium pressure at 80°C for a few days. The results of this "reheliumization" are indicated in figure 3-2. Although not indicated, the error bars on the points in figure 3-2 are such that there is no observable difference in xenon characteristics at 80°C for hydride and deuteride cells, whether one considers ^{131}Xe or ^{129}Xe. As the mass spectroscopy results showed that one deuteride cell had significantly less helium than the selected hydride cell, both types of systems were subjected to "reheliumization" studies. In spite of this, it was never possible to make the hydride and deuteride cells significantly different from each other for either xenon isotope.

Although comparisons of one temperature (80°C) have been found to be useful, they do not tell the whole story. During early stages of the aging process, between 1 and 2 weeks, temperature dependent data were taken and ^{129}Xe results fit to the form of equation (3.5) under the assumption that $\sigma\bar{v}$ and T_2' are constants over the temperature range of interest. This is consistent with current practice for these kinds of studies and allows for comparison with the work of other researchers (Ref 3-18). The results are presented in table 3-I. Results for different surface treatments are presented in section IV.

GUIDANCE & CONTROL SYSTEMS
5500 Canoga Avenue, Woodland Hills, California 91365

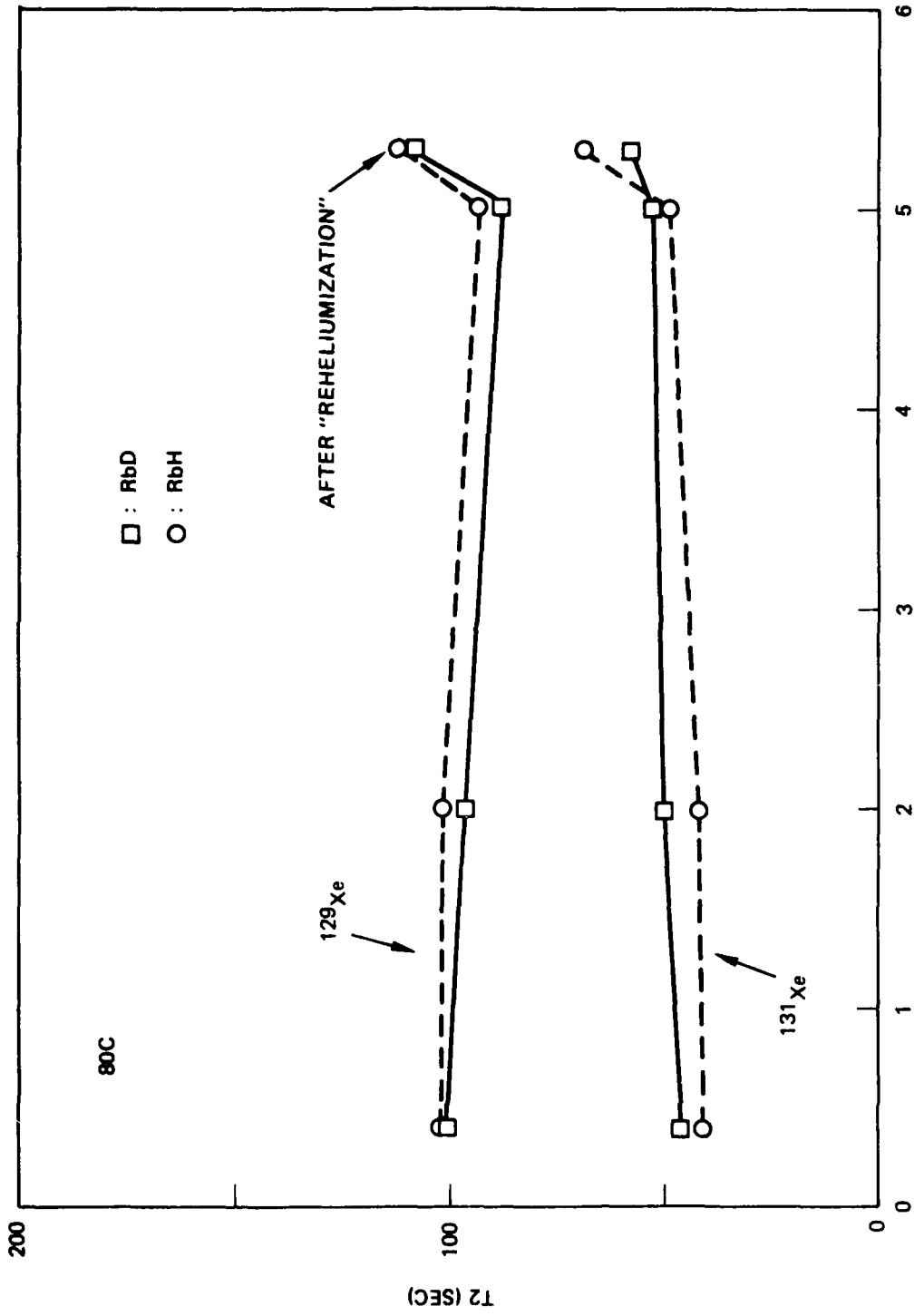

Figure 3-2. Effect of Helium Diffusion on NMR Cell Relaxation Times

GUIDANCE & CONTROL SYSTEMS
Litton 5500 Canoga Avenue, Woodland Hills, California 91365

TABLE 3-I. AVERAGE WALL RATE AND Rb DEPENDENT RATE FOR RbH AND RbD COATED CELLS FROM STUDIES OF ^{129}Xe TRANSVERSE RELAXATION

$\left(\frac{1}{T_2}\right)_{wall}$ (Sec^{-1})	$\sigma\bar{v}\left(\frac{cc}{\#Rb\ atoms\ sec}\right)$
Cells Coated with	
RbH $(2.48 \pm 0.37) \times 10^{-3}$	$(1.12 \pm 0.08) \times 10^{-14}$
RbD $(3.13 \pm 0.58) \times 10^{-3}$	$(1.10 \pm 0.05) \times 10^{-14}$

The data in table 3-I represent cells of approximately the same fill. The differences are 10 torr of H_2 or D_2 in the RbH or RbD cells. Within experimental error the gas phase results, represented by the parameter $\sigma\bar{v}$ are the same for both cell types. The RbH/RbD wall rates are also essentially the same. No amount of aging or helium treatments was capable of bringing out any marked difference between the deuteride and hydride cells. This is in sharp contrast to results found for other surface treatments. Taken together these results indicate that direct-dipole relaxation of ^{129}Xe on surfaces in cells of total gas pressure $\geq$ 100 torr is not important where the magnetic surface species is a nuclear spin.

Studies of various surface treatments now under way should help to characterize the nature of the mechanism controlling ^{129}Xe relaxation on surfaces in very low magnetic fields.

3.5 REFERENCES

3-1 B.C. Grover, Phys. Rev. Lett. 40, 391 (1978).

3-2 C.H. Volk, T.M. Kwon, and J.C. Mark, Phys. Rev. A 21, 1549 (1980).

3-3 N.D. Bhaskar, W. Happer, and T.M. McClelland, Phys. Rev. Lett. 49, 25 (1982).

3-4 E. Kanegsberg, H. Williams, B. Grover, J. Mark, NMR Gyro Study, Final Report for NAVAIR Contract No. N00019-75-C-0456 (March 1977). (Unpublished)

3-5 Physics Today, August 1982, pp 17-19.

3-6 M.A. Bouchiat and J. Brossel, Phys. Rev. 147, 41 (1966).

3-7 W.A. Fitzsimmons, L.L. Tankersley, and G.K. Walters, Phys. Rev. 179, 156 (1969).

3-8 W.A. Fitzsimmons and G.K. Walters, Phys. Rev. Lett. 19, 943 (1967).

3-9 C.P. Slichter, Principles of Magnetic Resonance, 2nd Ed. (Springer-Verlog, New York, 1978).

3-10 J.C. Tully, Surface Science 111, 461 (1981).

3-11 A.D. Zdetsis and A. Barry Kunz, Phys. Rev. B 26, 4756 (1982).

3-12 J.A. Cunningham, D.K. Greenlaw, and C.P. Flynn, Phys. Rev. B 22, 717 (1980).

3-13 T.M. Kwon, J.G. Mark, and C.H. Volk, Phys. Rev. A 24, 1894 (1981).

3-14 C.H. Volk, T.M. Kwon, J.G. Mark, Y.B. Kim and J.C. Woo, Phys. Rev. Lett. 44, 136 (1980).

3-15 A.T. Nicol, U.S. Air Force Office of Scientific Research Final Technical Report, Contract No. F49620-77-C-0047, 1982 (unpublished).

3-16 For a discussion of the rubidium magnetometer and the importance of rubidium in the alkali metal-noble gas system see reference 2.

3-17 C. Cohen-Tannoutjc, J. De Phys. 24, 653 (1963).

3-18 N.D. Bhaskar, W. Happer, M. Larsson, and X. Zeng, Phys. Rev. Lett. 50, 105 (1983).

Litton GUIDANCE & CONTROL SYSTEMS
5500 Canoga Avenue, Woodland Hills, California 91365

FSCM 06481

SECTION IV

EFFECT OF SEVERAL SURFACE TREATMENTS ON ^{129}Xe POLARIZATION AND RELAXATION IN NMR CELLS

4.1 INTRODUCTION

The importance of wall effects in polarization and relaxation of optically pumped spin systems has been pointed out by a number of people in the early days of optical pumping experiments, (ref. 4-1, 4-2) and has recently taken on new importance because of possible applications of gas phase nuclear polarization to enhanced fusion processes (ref 4-3). In a recent study, Optical Pumping of Dense Charge-Excharge Targets for Polarized Ion Sources, Cornelius et al (Ref 4-4) cited depolarizing effects of wall collisions as a deleterious effect. With the exception of one aspect of the ^{3}He studies (ref 4-1), consideration of wall effects has usually been directed toward studies of depolarization of the optically pumped species itself, i.e., the directly optically pumped He (as opposed to polarization through spin exchange) or the optically pumped alkali metal atom (e.g., Rb or Na). This section presents results in which the noble gas xenon is indirectly polarized through a spin exchange process (in which molecular formation plays an important part) and has a contribution to relaxation from that same process in addition to any wall effect present. This section presents the first systematic study of ^{129}Xe relaxing on a variety of surface types. It is hoped that the results will lead to more efficient and sustained polarization for a variety of systems.

4.2 THEORETICAL BACKGROUND

Nuclear spin relaxation of spin 1/2 systems was discussed in the preceding section. Specific results applicable to this study are restated here. Most generally the surface adsorption relaxation is given by

$$T_1 = \frac{N}{n} (\tau_s + T_s) \text{ for } n<<N \qquad (4.1)$$

and where τ_s is the average wall collision sticking time (or dwell time), and T_s is the characteristic relaxation time for the species, ^{129}Xe, on the surface. N is the number in volume V of atoms of the species under consideration, and n is the number of those atoms interacting with the surface at any instant. Under conditions outlined in the previous section the wall relaxation at the ith site can then be expressed by

$$T_{1i} = \frac{2V \; e^{-2E_i/kT}}{A\bar{v}_{xe} (\gamma_{xe}\bar{H}_{1i}\tau_s^o)^2} \qquad (4.2)$$

where T_{1i} is the relaxation time on the ith site, E_i is the surface binding energy of site i and H_{1i} is the local magnetic field at that site. V is volume, A is effective surface area (not necessarily apparent geometrical surface area), $\bar{v}_{xe}$ is the xenon atom mean velocity, and τ_s^o is the high temperature sticking time. The sticking time at site i, τ_{s_i}, at a given temperature T is given by

$$\tau_{Si} = \tau_s^o \; e^{E_i/kT} \; . \qquad (4.3)$$

It is usual to take τ_s^o as 10^{-12} sec, the approximate period of a molecular vibration and hence a good approximation for the break up time of a short lived complex on the surface. The effective local nuclear magnetic field was demonstrated in the previoius section not to be dominated by direct dipolar interactions due to nuclei on the surface containing non zero spins. The magnetic interaction then must be due to some other mechanism, for example, a larger magnetic moment due to an unpaired electron spin. Another possibility is that the alkali is efficiently depolarized at the surface and in turn depolarizes the noble gas nuclear

GUIDANCE & CONTROL SYSTEMS
Litton 5500 Canoga Avenue, Woodland Hills, California 91365
FSCM 06481

moment in a mechanism analogous to the gas phase interaction (Short lived Van der Waals molecule at the surface). As the surface/volume ratio is an important factor in equation (4.2) it would be unwise to overlook the fact that various surface treatments may influence the topography of the surface and in this way affect the relaxation time.

Although wall relaxation models have a clearly defined temperature dependence, in practice it is found that over the the temperature range typically studied (~50-100C) only a very weak temperature dependence is observed. The total relaxation rate can be expressed as

$$\frac{1}{T_2} = N_{Rb}\,\bar{\sigma v} + \frac{1}{T_2'} \qquad (4.4)$$

where T_2 is the transverse relaxation time, $N_{Rb}\bar{\sigma v}$ represents the gas phase rubidium density dependent relaxation rate, N_{Rb} is the rubidium number density, σ is the effective spin exchange cross section, and $\bar{v}$ is the xenon-rubidium relative velocity. T_2' represents all other relaxation effects. Repeated studies have shown that for cells of size and fill studied here the pump time and the transverse relaxation time are equal for ^{129}Xe (ref. 4-5). This indicates that field inhomogeneities are not an important source of relaxation in these systems and $1/T_2'$ may be considered to be a wall rate. For the studies presented here the simple form given by equation (4.4) was used.

4.3 EXPERIMENT

Six sets of cells with various surface treatments containing ^{87} Rb and very nearly the same gas fill were produced. The nominal gas fill is 0.5 torr ^{129}Xe, 2.5 torr ^{131}Xe, 40 torr N_2 100 torr He, and 0-10 torr H_2. Each set consisted of six cells prepared on one manifold on the vacuum stand.

Litton GUIDANCE & CONTROL SYSTEMS
5500 Canoga Avenue, Woodland Hills, California 91365

Initially, three of the sets were prepared using pyrex glass, attached to three separate parts of the vacuum line, baked out over night, and filled the next day. One set contained no hydrogen, the second had 10 torr added H_2 and the third had 10 torr added D_2. A surface coating forms readily in cells with H_2 and D_2. In this study the sets are referred to as plain pyrex, pyrex/RbH, and pyrex/RbD cells. The RbH and RbD cells are the same cells discussed in section III.

Subsequently a set of silicone surface treated pyrex cells was prepared. Prior to attachment to the manifold, the six cells were chemically cleaned. Following that the cells were treated with 10% Surfasil (Pierce Chemical Co.) in acetone, dried and cured at 100°C and attached to the manifold for filling. The cell gas fill was the same as for the plain pyrex cells.

After testing, selected cells from pyrex/RbD, pyrex/RbH and pyrex/silicone were sent for destructive testing of gas fill by means of mass spectroscopy. The results of the destructive testing indicated that, with the exception of a certain amount of helium loss due to aging, the fill station results are fairly accurate. Yet the observed $^{129}Xe/^{131}Xe$ signals varied sufficiently to warrant developing a better technique for detailed surface comparisons. In an effort to minimize gas phase differences and thereby point up surface differences, a research gas mix was prepared from 60% enriched ^{129}Xe and ^{131}Xe, and buffer gases N_2 and He. Several samples of the resulting mix were analyzed by mass spectroscopy and found to contain 0.3% ^{129}Xe, 1.9%, ^{131}Xe, 29% N_2 and 60% He.

Two sets of cells containing the research gas mix were then prepared. The first set was pyrex and was filled with 10 torr H_2 plus 143 torr of research mix. This corresponds closely to the previous cell fills used in this study. The second set was prepared from high purity quartz. The cells were ultrasonically cleaned with deionized water and then heat treated in air at 700°C

for 48 hours. The treatment has a surface annealing effect (ref. 4-6) which was thought possibly beneficial to xenon relaxation properties. In addition, advantage might be gained from use of high purity materials. On the other hand, quartz has very poor characteristics as far as helium diffusion and rubidium attack are concerned. The cells were prepared with those characteristics in mind. Ample rubidiium was used and the cells were prepared with thick walls. Three of the six cells were filled with 143 torr of research mix, and the other three were filled with ten torr of H_2 and 143 torr of research mix.

All six sets of cells described here were studied as a function both of aging time and, periodically, as a function of temperature in an NMR apparatus which has been described in the literature (ref 4-7).

4.4 RESULTS AND DISCUSSION

Transverse relaxation time data as a function of temperature were taken on cells aged, typically, for 2-4 weeks. As discussed in section III, pyrex cells will lose a significaant amount of helium during aging at 80°C. Efforts were made to keep the studies "parallel" in the sense that cells were treated to similar times in the rubidiium rearrangement oven or in the aging oven. Typically, cells are placed in the oven for 2 to 3 days at 100-130°C with a cold finger at the tip-off region of the cell. The temperature differential drives rubidium metal into the tip-off region. The cell is then placed in an aging oven at 80° C for a time period extending from a few days to several weeks. Careful monitoring of the NMR characteristics at 80°C as a function of aging not only pointed up the potential loss of helium, later confirmed independently by mass spectroscopy, but also showed that the cells are almost sufficiently aged by the time the rubidium rearrangement process is completed.

Data regarding the temperature dependence of ^{129}Xe relaxation times, T_2, were taken for similarly treated cells. For each individual cell the data were fit to the function form of equation (4.5)

$$\frac{1}{T_2} = N_{Rb}\sigma\bar{v} + \frac{1}{T'_2} \quad . \qquad (4.5)$$

The assumption was made that $1/T'_2$ is constant over the temperature range of interest. The values obtained for $1/T'_2$ and $\sigma\bar{v}$ for the cells within each set were quite consistent. The average of those results and the standard deviation are presented in table 4-I. The data for the pyrex/RbH and pyrex/RbD represent averages for six cells per set while only two of the plain cells are represented in the table. Wall rates for the remaining plain cells taken after much aging cannot be directly compared with the results in table I but were consistent with those results. They exhibited gas phase rates typical of less buffer fill (He loss) and wall rates comparable to data in table 4-I. The data for the pyrex/RbH/research mix cells represent results for four of six cells. The other two were used for independent analysis of gas fill.

Although no data are presented in table 4-I for the quartz cells they present some results not seen previously with pyrex or Corning 1720 glass. For the plain (non hydrogen containing) quartz cells the wall rates for ^{129}Xe appear comparable to those found for plain pyrex (cf table 4-I). The results for ^{131}Xe, on the other hand, are markedly different from those found for plain pyrex.

Whereas plain pyrex cells exhibit short ^{131}Xe relaxation times as well as low signal amplitude, the plain quartz cells show ^{131}Xe relaxation times and signed amplitudes similar to those found in RbH coated pyrex cells. These interesting results are being followed up with a long term aging study in which the helium cell fill is maintained through use of a known external helium pressure.

GUIDANCE & CONTROL SYSTEMS
5500 Canoga Avenue, Woodland Hills, California 91365
FSCM 06481

TABLE 4-I. AVERAGE WALL RATE AND Rb DEPENDENT RATE FOR VARIOIUS TYPES OF CELLS FROM STUDIES OF ^{129}Xe TRANSVERSE RELAXATION

	$\left(\frac{1}{T_2}\right)_{wall}$ (sec^{-1})	$\sigma\bar{v}\left(\frac{cc}{\#Rb\ atoms\ sec}\right)$
Plain Pyrex	$(3.11 \pm .28) \times 10^{-2}$	$(7.42 \pm 2.92) \times 10^{-15}$
Pyrex Cells Coated with		
RbH	$(2.48 \pm 0.37) \times 10^{-3}$	$(1.12 \pm 0.08) \times 10^{-14}$
RbD	$(3.13 \pm 0.58) \times 10^{-3}$	$(1.10 \pm 0.05) \times 10^{-14}$
Silicones	$(1.10 \pm 0.38) \times 10^{-3}$	$(1.03 \pm 0.06) \times 10^{-14}$
Cells Filled with Research Mix:		
Pyrex Coated With RbH	$(3.37 \pm 1.09) \times 10^{-3}$	$(1.05 \pm 0.11) \times 10^{-14}$

Interestingly, the quartz cells seem to present a more reactive surface than plain Pyrex or Corning 1720 glass. All hydrogen containing cells reacted to completion consuming all rubidium metal within a few weeks. Prior to that, the hydrogen containing cells exhibited NMR parameters (^{129}Xe and ^{131}Xe signal amplitudes and relaxation terms) generally inferior to comparable pyrex/RbH cells.

These results suggest that, although pure silica is probably a poor material for long lived gyro cells, it may be a useful tool for surface studies.

Referring again to table 4-I, the results show, within experimental error, that all cells with the same gas fill exhibit the same gas phase rate as expected. The wall rates, however, can be very different. Note that the wall rate for the plain pyrex cells is an order of magnitude larger than the RbH/RbD or the research

mix/RbH cells which, in turn, exhibit a factor of 3 larger wall rate than the silicone surface treated cells. Repeated efforts to find a significant difference between RbH and RbD surface treated cells indicate that there is no difference as far as ^{129}Xe relaxation is concerned. It should be noted that such studies have not been presented previoiusly. It has been the experience of workers in this field that it was not possible to get consistent results within a single set of cells. Through development of careful production techniques this problem has been overcome. This is evident in the statistics presented in table 4-I.

At this time further studies are being carried out in an effort to characterize fully the surface types. The results presented here are inadequate to provide any interpretation regarding the thickness or topology of the walls. Important questions exist regarding both. To the extent that paramagnetic sites in the glass may be effective in relaxing the nuclear spin (nuclear moments are not very effective) it is beneficial to maximize the distance between the noble gas nucleus and the unpaired electron. This follows from the fact that the relaxation rate varies as $1/r^6$, where r is the interspin distance. Thus wall coating thickness can be important. From equation (4.2) it is evident that the effective surface/volume ratio can be important. Hence the topology can effect the relaxation times. It is also very likely that relaxation occurs through an electron-nuclear interaction such as indirect nuclear coupling or even a spin orbit interaction at the surface (ref 4.8). This is still a magnetic mechanism. The difference is that $\bar{H}_1$ depends on the angular momentum of an effective unpaired spin density or a surface-formed Van der Waals molecule.

These initial NMR wall relaxation studies are encouraging. Studies continue aimed at finding methods to characterize better wall coatings by independent testing. Further types of wall coatings are under investigation and it is hoped that these studies will lead to enhanced gas phase nuclear polarizations.

4.5 CONSIDERATION FOR FUTURE WORK

The results presented in Sections III and IV demonstrate the importance of surface treatment in NMR cells as far as ^{129}Xe is concerned. Further work is needed to characterize fully wall relaxation effects on ^{131}Xe. The achievement of surface treatments which give repeatable and reproducible results indicates that benefits in NMR cell performance may be obtained through extention of the investigation to other methods of surface treatment. The treatments under consideration include (1) bonding of surfactants to the cell surface and (2) chemical cleaning treatments known to reduce effective surface area. In conjunction with the surface treatments, plans are underway to investigate the effects of other buffer gas mixes (e.g., N_2/He/Ne) on both the gas phase and wall relaxation characteristics. The latter becomes important as increased buffering affects both the surface sticking time and the rubidium polarization gradient near the surface. Experiments will lead to a better characterization of the details of gas phase and surface noble gas nuclear relaxation in very low magnetic fields.

4.6 REFERENCES

4-1. W.A. Fitzsimmons, L.L. Tankersley, and G.K. Walters, Phys. Rev. 179, 156 (1969).

4-2. M.A. Bouchiat and J. Brossel, Phys. Rev. 147, 41 (1966)

4-3. Physics Today, August 1982, pp 17-19.

4-4. W.D. Cornelius, D.J. Taylor, R.L. York, and E.A. Hinds, Phys. Rev. Lett. 49, 870 (1982).

4-5. A.T. Nicol, U.S. Air Force Office of Scientific Research Final Technical Report, Contract No. F49620-77-C-0047, 1982 (unpublished).

4-6. J.A.G. Taylor, J.A. Hockey, and B.A. Pethica, Proc. Brit. Ceram. Soc. 5, 133 (1965).

4-7. C.H.Volk, T.M. Kwon, and J.G. Mark, Phys. Rev. A 21, 1549 (1980).

4-8. R.M. Hermon Phys Rev. A 25, 1383 (1982).

4-9. A.D. Zdetsis and A.B. Kunz, Phys. Rev. B 26, 4756 (1982).

GUIDANCE & CONTROL SYSTEMS
5500 Canoga Avenue, Woodland Hills, California 91365

SECTION V

XENON NUCLEAR POLARIZATION AND RELAXATION IN DUAL ALKALI CELLS

5.1 INTRODUCTION

An important question in NMR gyro operation is that of turn-on time. Directly related to this is the fundamental physics dictating the time needed to create detectable noble gas nuclear polarization in the sample cell. Characteristic polarization pump times in alkali metal-noble gas systems are known to depend on the alkali metal vapor density. A series of experiments involving dual alkali cells containing rubidium and cesium were undertaken to evaluate noble gas pumping rates as a function of alkali metal vapor densities.

For the case of a cell with the single alkali, rubidium, the spinning-up, or pump time, of Xe is given by

$$\frac{1}{T_p} = \frac{1}{T_1} + N_{Rb}\ \sigma\ \bar{V} \qquad (5.1)$$

where T_1 is the relaxation time due to magnetic field inhomogeneity and wall effects, N_{Rb} is the Rb density, $\bar{V}$ the average collision velocity between Rb and Xe, and σ is the effective spin-exchange cross-section. From equation, (5.1), it is seen that the pump time T_p is shortened by increasing the Rb density, N_{Rb}. However, the bias drift of an NMR gyro varies as

$$B\ \alpha\ \frac{1}{\sqrt{T_p\ T_2}}$$

where T_2 is the transverse relaxation time (and generally $T_2 \leq T_p$), a short T_p would degrade gyro performance. A large N_{Rb} would also make the Rb vapor too optically thick for the Rb pump light to penetrate and for the detection light to be monitored. The operating temperature of the Rb-Xe Demonstration Model Gyro (DMG)

GUIDANCE & CONTROL SYSTEMS
Litton 5500 Canoga Avenue, Woodland Hills, California 91365

optimized for S/N and bias drift is between 70°-80°C, with a pump time of 100-200 s. A simple solution to fast spin-up of the Xe is to create an unusually large alkali metal vapor density during the initial turn-on period of the gyro when detection light does not have to be monitored and the bias drift is of no concern. The purpose of this investigation is to study such an approach. More specifically, the question of whether the pump rate T_p^{-1} scales up with N_{Rb} according to equation (5.1) in the optically dense regime is asked.

5.2 EXPERIMENT

A study of the spin-exchange process between an alkali vapor and a noble gas in the optically thick regime would appear to exclude the use of the optical means of monitoring. This difficulty is circumvented by using a cell containing both Rb and Cs. Since the vapor presence of Cs is roughly six times that of Rb, the Cs vapor can be optically thick without the Rb vapor being so. An Rb lamp is used to pump the Rb atoms, which polarize the Cs atoms by spin-exchange in a few milliseconds due to the large spin-exchange cross section between Rb and Cs ($\sim 2 \times 10^{-14}$ cm^2). The Xe nuclei are then polarized at a slower rate (in ~ 10-100 s) by both the Rb and Cs atoms.

Several DMG size cells were prepared with gas fills of 80 torr He, 40 torr N_2, 1 torr ^{129}Xe, and a mixture of distilled ^{87}Rb and ^{133}Cs in the ratio of 1:1 (cells No. 376 and No. 377) and 1:2 (cell No. 375 and No. 378,) respectively. The partial vapor pressures of Rb and Cs in a molar ratio of x:y are assumed to be given by Raoult's Law. The densitites of the rubidium and cesium will then be

$$N_{Rb} = N^o_{Rb}\, x/(x+y) \tag{5.2}$$

and

$$N_{Cs} = N^o_{Cs}\, y/(x+y) \tag{5.3}$$

Where N°_{Rb} and N°_{Cs} are the densities of pure Rb and Cs separately. Since Raoult's Law is not precise for high mixing ratios and the actual mixing ratio of alkalis distilled into a cell is only a rough estimate, the number densities of the mixed alkalis at a particular temperature is approximate as determined from equations (5.2) and (5.3).

The experimental apparatus and the general experimental procedure as well as the use of the rubidium magnetometer for detecting the precessing noble gas nuclear moments have been described previously (ref 5-1).

5.3 RESULTS AND DISCUSSION

5.3.1 Spin Exchange Between Rb, Cs and Xe. A series of experiments established that spin exchange takes place between the Rb-Cs and between the alkali-xenon systems. In the first experiment, a ^{87}Rb lamp was used to pump cell No. 375. In such experiments the pump light is along the x-direction as defined in Ref. (5-1) and passed through a D_1 filter and a circular polarizer. After passing through the cell, the transmitted light is monitored by a detector. An 8 kHz RF magnetic field is applied in the z-direction. Figure 5-1(a) shows the transmitted light intensity as the x magnetic field is swept across the Rb magnetic resonance at 11.4 mG. Figure 5-1(b) shows Cs resonance at 22.8 mG. This establishes that cesium is polarized through spin exchange with the optically pumped rubidium present in the system. The magnetic field is then changed to a non-resonant value and the cell is allowed to be pumped for a few minutes. The x-field is suddenly removed and a y-field of ~ 150 μG is applied. The transmitted light, after demodulation at 8 kHz, is shown in figure 5-1(c). The oscillation represents precession of the Xe nuclear moment about the y-field and the exponential envelope represents the transverse relaxation time T_2. The data in figure 5-1 are taken at 73.8°C. NMR signals can be observed with Rb pump light with

Litton GUIDANCE & CONTROL SYSTEMS
5500 Canoga Avenue, Woodland Hills, California 91365

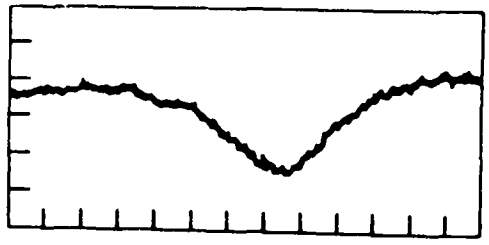

(a) TRANSMITTED Rb PUMP LIGHT VS H_X. Rb RESONANCE AT 11.4 mG AND 8 kHz

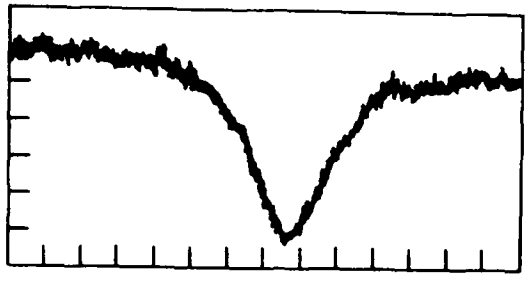

(b) Cs RESONANCE AT 22.8 mG AND 8 kHz

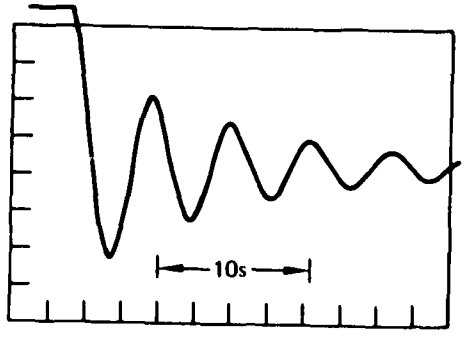

(c) DEDMODULATED 8 kHz SIGNAL. Xe NUCLEAR PRECESSION

Figure 5-1. Spin-Exchange Between Rb, Cs and Xe

cell temperature of 65°C-110°C. Below 65°C, the partial pressure of Rb is too low to produce a good NMR signal. Above 110°C, the vapor becomes too optically thick for Rb as well as Cs light. The results above show that Xe can be polarized by a mixture of Rb and Cs at high densities.

5.3.2 Traverse Versus Longitudinal Relaxation of ^{129}Xe. At high alkali densities, most of the relaxation of Xe polarization is due to spin-exchange with the alkalis and it is expected that $T2 \approx T_p$. T_2 and T_p were measured at different temperatures to verify this relationship. T_2 was measured from an exponential envelope such as that shown in figure 5-1(c). T_p was measured from the initial amplitude of the ^{129}Xe precision curve as a function of pump time. The data for cell #375 at the temperature of 73.8°C are fitted in figure 5-2 with T_2 = 16.0 s and in figure 5-3 with T_p = 16.2 s. These results are completely consistent with results for ^{129}Xe in rubidium single alkali systems (ref 5-2). As T_2 is more easily determined than T_p, T_2 is used as an indicator of the pump time.

5.3.3 Comparison of Cells with Different Rb:Cs Ratios. The optical pumping results for cells with different mixing ratios of Rb:Cs pumped by the same Rb lamp in the same apparatus at ~ 70°C are tabulated in table 5-I. Cell No. 266 is a Rb cell without any Cs and was selected from a large set of cells for long relaxation time. That accounts for the difference in T_2 between No. 266 and the other two cells, although increased Cs density also contributes to shortening the T_2. A more detailed modeling is required to interpret quantitatively the results in table 5-I. However, the effect of the higher vapor pressure of Cs is seen from the trend of change of the different parameters in table 5-I. The Rb relaxation as measured by $1/\tau$, the Rb linewidth, increases with Cs admixture due to Rb-Cs spin-exchange, which also accounts for a decrease in Rb polarization. The decrease in T_2 and H_{Xe}, the magnetic field due to Xe magnetization, is mainly due to the

intrinsic higher wall relaxation of the dual alkali cells which have not been specially selected or coated for low wall relaxation.

TABLE 5-I. COMPARISON OF CELLS WITH DIFFERENT Rb:Cs RATIOS

Cell	Rb:Cs	Temp	Rb.POL.	H_{Xe}	T_2	τ	τ_p
266	1:0	70.0°C	8.3%	22 μG	132 s	1.8 ms	3.3 ms
377	1:1	73.8°C	5.1%	5.7μG	19.5 s	1.2 ms	4.5 ms
365	1:2	73.2°C	5.1%	3.3μG	16 s	1.1 ms	3.6 ms

5.3.4 Relaxation Rate Versus Alkali Density. To measure the wall relaxation of Xe, as has been explained in detail in Section III, T_2 must be extrapolated to the zero alkali density limit. As the NMR signal in the Rb-Cs cells is too weak with Rb light pumping at temperatures below ~ 65°C, the low temperature T_2 measurements were made with a Cs lamp directly pumping the major alkali constituent, Cs. A plot of T_2^{-1} vs the alkali density for cells No. 266 (Rb:Cs = 1:0) and No. 376 (Rb:Cs = 1:1) is shown in figure 5-4. For cell No. 376, the total alkali density is estimated from Raoult's Law, equations (5.2) and (5.3). The wall relaxation time, as given by the y-intercept, is ~200 s for No. 266 and ~57 s for No. 376. For cell No. 266, the NMR signal becomes too weak to measure for $N_{Rb} \leq 3 \times 10^{12}$ cm^{-3} (100°C). The combined Cs and Rb density for No. 376 at the same temperature is ~ 9×10^{12} cm^{-3}. Figure 5-4 shows that the dual alkalis have approximately the same average relaxation cross section as rubidium (~2×15^{-19} cm^2) and the relaxation rate scales linearly up to a density of almost 10^{13} cm^{-3}. Note that the data for cell No. 376 in figure 5-4 are limited to an alkali density of less than 10^{13} cm^{-3} above which even the minor constituent, Rb, becomes optically thick. Higher alkali densities could be explored using a Cs-K mixture with a larger vapor density difference. The dual alkali cell serves well as a research probe into the higher alkali density regime. The results of this study have lead to new concepts for fast gyro turn-on.

Litton GUIDANCE & CONTROL SYSTEMS
5500 Canoga Avenue, Woodland Hills, California 91365

FSCM 06481

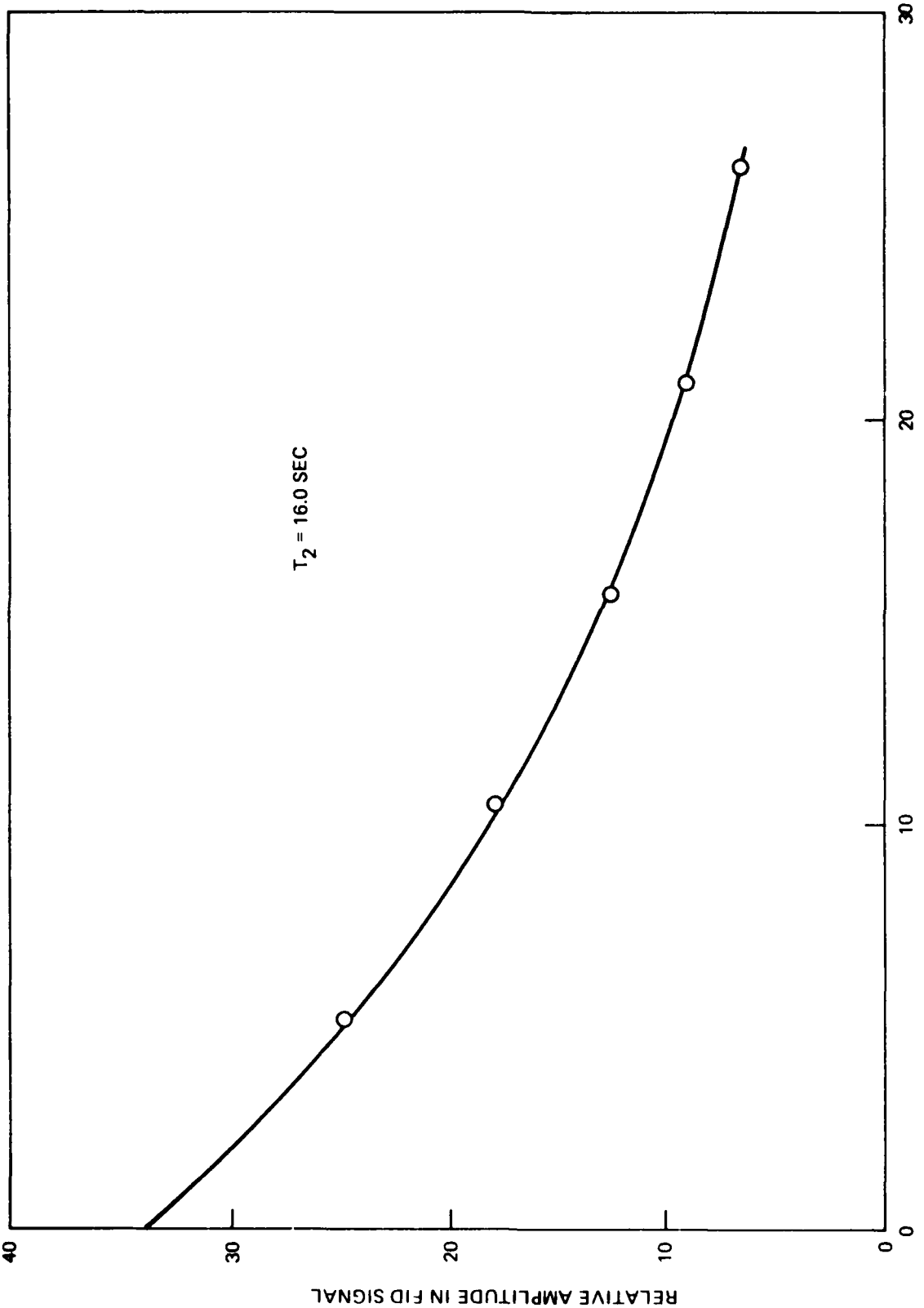

Figure 5-2. Fitted T_2 Decay Curve for Cell No. 375 at 73.8°C

Litton GUIDANCE & CONTROL SYSTEMS
5500 Canoga Avenue, Woodland Hills, California 91365

FSCM 06481

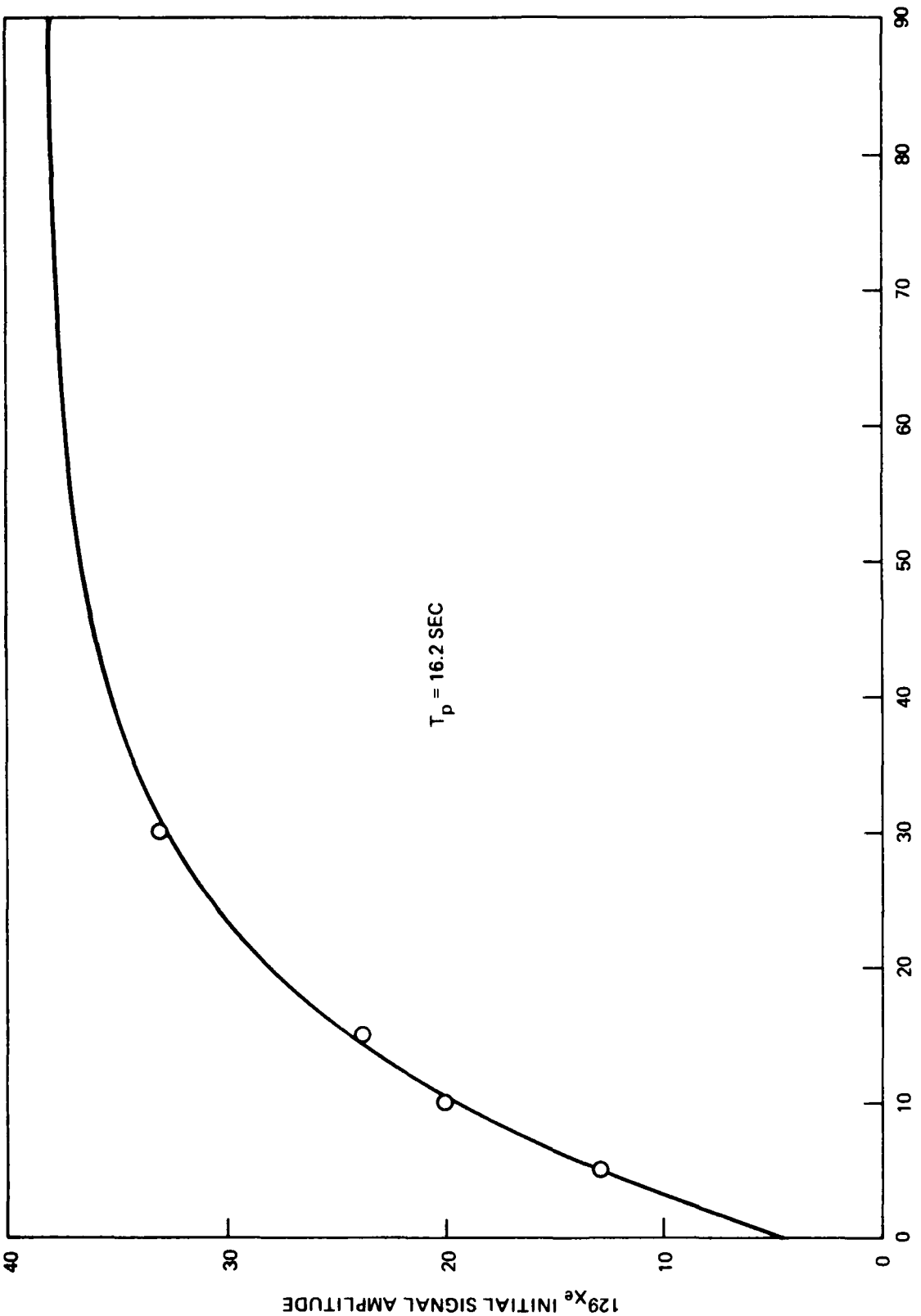

Figure 5-3. Fitted T_p Curve for Cell No. 376 at 73.8°C

Litton GUIDANCE & CONTROL SYSTEMS
5500 Canoga Avenue, Woodland Hills, California 91365

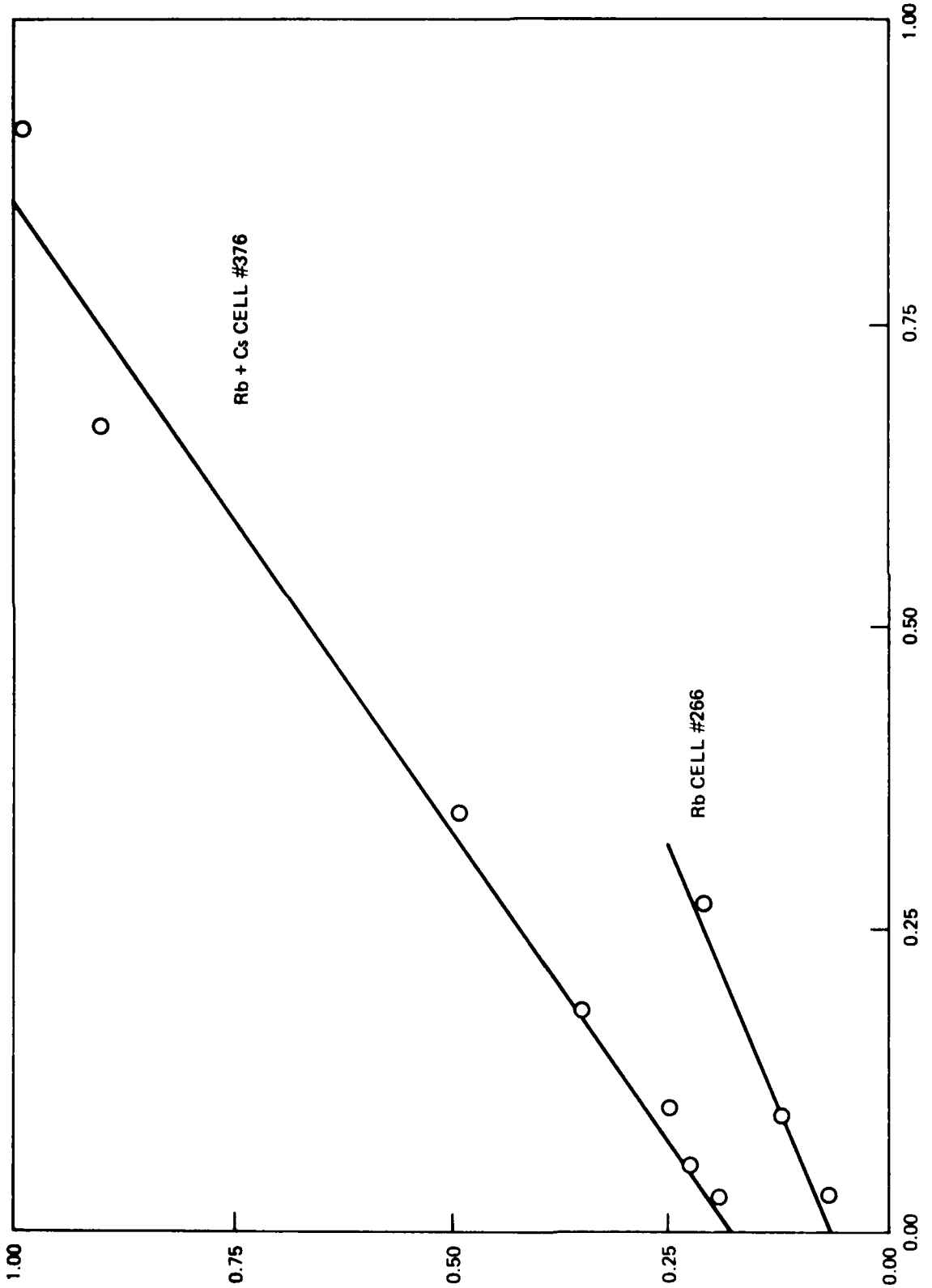

Figure 5-4. $1/T_2$ vs $N_{Rb} + N_{Cs}$

5.4 REFERENCES

5-1. C.H. Volk, T.M. Kwon, and J.G. Mark, Phys. Rev. A 21, 1549 (1980).

5-2. A.T. Nicol, U.S. Air Force Office of Scientific Research Final Technical Report, Contract No. F49620-77-C-0047, 1982 (unpublished).

GUIDANCE & CONTROL SYSTEMS
Litton 5500 Canoga Avenue, Woodland Hills, California 91365

FSCM 06481

SECTION VI

OPTICAL PUMPING OF Rb WITH A TURNABLE LASER DIODE

6.1 INTRODUCTION

Optical pumping of Rb with a CW, single-moded laser diode differs from pumping with a Rb resonance lamp. The difference is due to the mismatch of emission and absorption spectral profiles. In the limit of low Rb vapor density and high pump light intensity, the pumping rate dominates the spin-exchange rate. The monochromatic pump light interacts only with Rb atoms in one depleted hyperfine level. The pump light can be more efficiently utilized by increasing the Rb vapor density and hence the spin-exchange rate. However, in a Rb-Xe gyroscope, increased Rb density would shorten the transverse relaxation time of the Xe nuclei. We examine here the electronic spin polarization $\langle S_z \rangle$ produced in an alkali vapor, in the absence of spin-exchange, when only one of its hyperfine level in the ground state is optically pumped.

6.2 RATE EQUATION MODEL

In a rate equation model of optical pumping figure 6-1, we consider the ith sublevel (i = 1 to N) in the ground state with pumping rate P_i , relaxing rate R_{ij} from $|i\rangle$ to $|j\rangle$ and a quenching rate Q_i from excited state $|e\rangle$ to $|i\rangle$. Because of the rapid depolarization and mixing in the excited ^2P state, the sublevel structure of the excited state does not have to be considered. The rate equations are, for i = 1 to N,

$$\frac{dn_i}{dt} = -P_i n_i - \sum_j R_{ji} n_i + \sum_j R_{ij} n_j + Q_i n_e \qquad (6.1)$$

and

$$\frac{dn_e}{dt} = -\sum_i Q_i n_e + \sum_i P_i n_i \qquad (6.2)$$

GUIDANCE & CONTROL SYSTEMS
Litton 5500 Canoga Avenue, Woodland Hills, California 91365

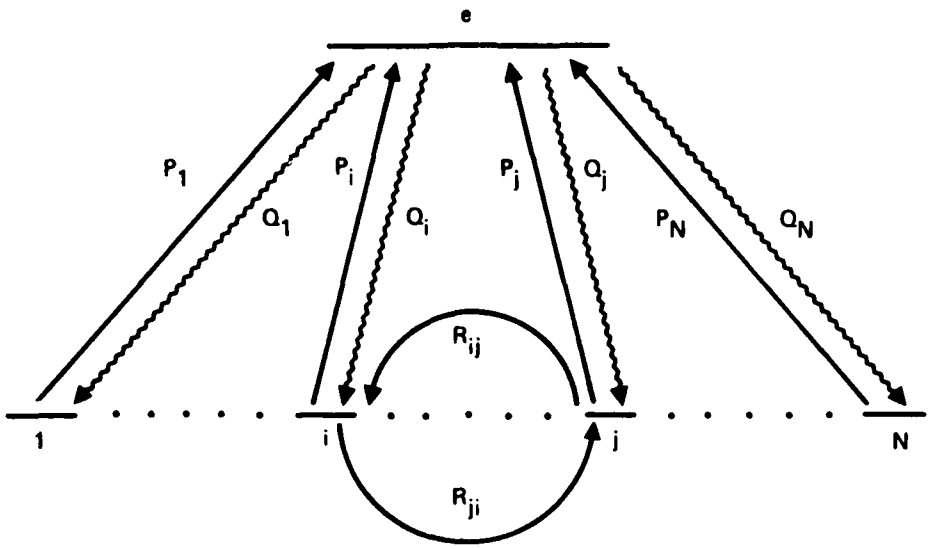

Figure 6-1. Optical Pumping Rate Equation Model

Conservation of atoms yields

$$\sum n_i = n_o - n_e \simeq n_o \qquad (6.3)$$

since $n_e << n_o$ when the pump rates P_i are much smaller than the quenching rates Q_i.

At steady state,

$$\frac{dn_i}{dt} = \frac{dn_e}{dt} = o \qquad \text{for } i = 1 \text{ to } N,$$

so that we have

$$n_e = \sum_i P_i n_i / \sum_i Q_i .$$

Substituting into (6.1) gives

$$\left(-P_i - \sum_j R_{ji} + \frac{Q_i P_i}{\sum_j Q_j}\right) n_i + \sum_j \left(R_{ij} + \frac{Q_i P_j}{\sum_k Q_k}\right) n_j = 0. \qquad (6.4)$$

Equations (6.3) and (6.4) can be readily solved for the population in the different sublevels n_i when the pumping, relaxation and quenching rates are known.

In the alkali ground state, all the ground state sublevels are nearly degenerate compared to the thermal Boltzmann factor so that

$$R_{ij} = R \text{ for all } i \neq j$$

In the presence of nitrogen in the buffer gas, excited state quenching is mostly non-radiative and random, so that

$$Q_i = Q \text{ for all } i$$

Equation (6.4) then simplifies to

$$-(N-1)\left(\frac{Pi}{N} + R\right) n_i + \sum_{j=i} \left(\frac{Pj}{N} + R\right) n_j = 0 \qquad (6.5)$$

However, depending on the amount of N_2 and the excited state lifetime, there may not be enough coupling of the nuclear and electronic spin in the excited state and only the electronic spin is randomized by the N_2 gas (ref. 6-1). This means that the Q_i's can be different and have to be obtained by properly projecting the nuclear spherical tensor moments T_{LM} (I I) onto tensor basis operators in terms of the total spin F, T_{LM} (FF).

When the population in the different hyperfine sublevels, $n(F, m_F)$, is calculated, the electron spin polarization $\langle S_z \rangle$ can be obtained as

$$\begin{aligned}
\langle S_z \rangle &= \sum_{m_s, m_I} m_s \langle Im_I \; Sm_s | \rho | Im_I \; Sm_s \rangle \\
&= \sum_{m_s m_I F m_F F' m_F'} m_s \langle Im_I \; Sm_s | Fm_F \rangle \langle Fm_F | \rho | Fm_F' \; m_F' \rangle \langle F' m_F' | IM_I Sm_s \rangle \\
&= \sum_{m_s F_{mf}} m_s | \langle I, m_F - m_s, S, m_s | F, m_F \rangle |^2 \; n(F, m_F) \\
&= \sum_{F m_s m_F} m_s \; C^2 (ISF; m_F - m_s, m_s, m_F) \; n(F, m_F), \qquad (6.6)
\end{aligned}$$

GUIDANCE & CONTROL SYSTEMS
Litton 5500 Canoga Avenue, Woodland Hills, California 91365

FSCM 06481

where C is the Clebsch - Gordon coefficient.

Application of the model to the $F_g = 2$ to $F_e = 1$ and $F_e = 2$ hyperfine pumping of the D1 line on ^{87}Rb ($I = 3/2$), as illustrated in figure 6-2, requires knowledge of the coefficient P_i, R_i and Q_i in equation (6.4). The solution is straightforward but tedious and can be shown to have the following functional form

$$\langle S_z \rangle_{F_g = 2} = a \frac{P\, P_{n-1}(P,R)}{P_n(P,R)} \tag{6.7}$$

where P and R are some averaged pump and relaxation rates that are respectively proportional to the pump light intensity and buffer gas densities. $P_n(P,R)$ is an nth order polynomial in P and R of the form,

$$P_n(P,R) = P^n + b_1 P^{n-1} R + b_2 P^{n-2} R^2 + \ldots + b_n R^n \,. \tag{6.8}$$

Similarly, the solution for the pumping of the $F_g = 1$ to the combined $F_e = 1$ and $F_e = 2$ states can be expressed as

$$\langle S_z \rangle_{F_g = 1} = a' \frac{PP'_{n-2}(P,R)}{P'_n(P,R)} \tag{6.9}$$

Equations (6.8) and (6.9) can be compared with the solution for the case when both hyperfine levels are pumped by a broadband light source so that the nuclear spin can be neglected,

$$\langle S_z \rangle_{J_g = \frac{1}{2}} = \frac{1}{2} \frac{P}{P+R} \tag{6.10}$$

The limiting cases of very strong or very weak pump intensity can be easily calculated for equations (6.7) and (6.8). When $P >> R$, $\langle S_z \rangle_{F_g = 2}$ approaches 1/8 which implies $a = 1/8$ in equation (6.7).

GUIDANCE & CONTROL SYSTEMS
Litton 5500 Canoga Avenue, Woodland Hills, California 91365

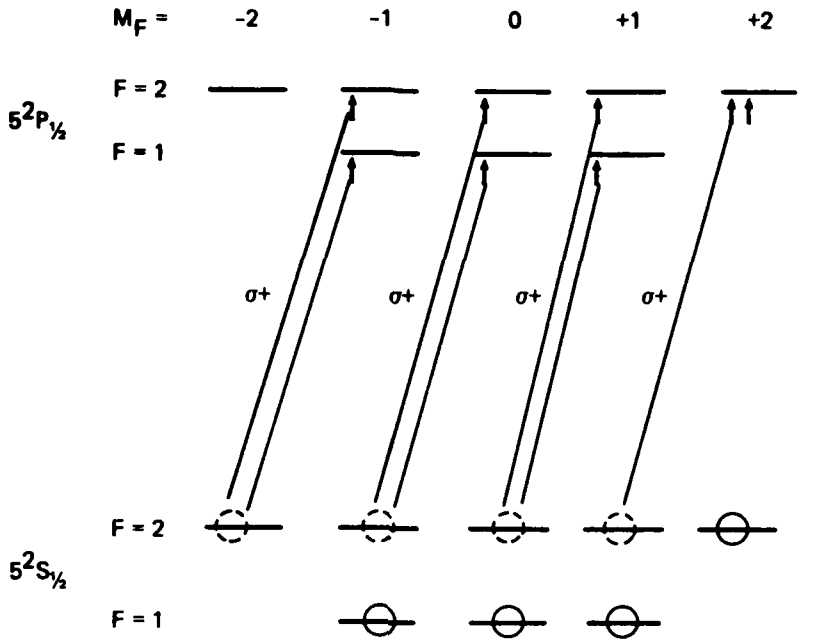

Figure 6-2. Hyperfine Pumping Levels

The difference of a factor of 4 between equations (6.7) to (6.10) can be understood with reference to figure 6-2. When both hyperfine lines are strongly pumped by σ+ light, only the F = 2, M_F = +2 state remains populated, with a spin polarization of $\langle S_z \rangle$ = 1/2. When only the upper hyperfine component is pumped, all three sublevels of the F = 1 line remain undepleted and relaxation and quenching tend to equalize their population. Since the unpolarized F = 1 state has $\langle S_z \rangle$ = 0, the net $\langle S_z \rangle$ for the ground state is 1/8. Similar arguments yield a spin polarization of $\langle S_z \rangle$ ≈ 0 for P>>R when only the F_g = 1 component is pumped, as shown by equation (9).

In the case of weak pumping, i.e., P << R, the electronic spin polarization can be expressed as

$$\langle S_z \rangle = Tr\ (PS_z) = -Tr\ (\delta\Gamma\ S_z)/\ (2F_g+1)R \qquad (6.11)$$

where repopulation pumping is neglected and

$$\delta\Gamma = 3R\,(F_g,F_e)(2F_g+1)W(1,1,F_e,F_g;\,1F_g)E_{10}T_{10}(F_gF_g)$$

and

$$R(F_g,F_e) = 2\lambda r_o c f_{ge} u(2h)^{-1}\, W^2(\tfrac{1}{2},\, F_e,\, \tfrac{1}{2},\, F_g;\, \tfrac{3}{2},\, 1)(2F_e+1)$$

Notations used are the same as those in Section III A of ref 6-2. Retaining only terms containing F_e and F_g,

$$\langle S_z\rangle \propto \frac{1}{F_g(2F_g+1)(F_g+1)} \sum W^2(\tfrac{1}{2},\, F_e,\, \tfrac{1}{2},\, F_g;\, \tfrac{3}{2},\, 1)W(1,\, 1,\, F_e,F_g;\, 1,\, F_g)$$

$$X\ \mathrm{Tr}(F_zS_z)\ \frac{P}{R}$$

$$\propto \begin{matrix} -1.89 \times 10^{-3}\ P/R \text{ for } F_g = 1 \\ 1.033 \times 10^{-2}\ P/R \text{ for } F_g = 2 \end{matrix} \qquad (6.12)$$

In our experiment, we used a cw GaAlAs laser diode of Mitsubishi model ML-5340 with an output of ~ 2 mW. The spectral profile was checked with a Fabry-Perot interferometer to be single-moded and of a width ~700 MHz. The laser was temperature tuned to the D1 line wavelength of Rb at 795 nm and then current tuned by ramping the injection current with the temperature held constant. The output beam was directed into the pumping channel of a NMR gyro module (the developmental module gyro, DMG) while the Rb polarization was monitored with a cross-beam from a resonance Rb lamp. The Rb cell, heated to 75°C, contained 100 torr of He, 10 torr of N_2 and 1 torr of ^{129}Xe. A test AC field of 25 Hz was fed to the sensitive axis of the DMG as a magnetometer. Preliminary data of the magnetometer sensitivity is plotted in figure 6.3. The magnetometer sensitivity is proportional to the Rb spin polarization $\langle S_z\rangle$, since the probing crossbeam is broadbanded. The laser

frequency was scanned over the hyperfine lines c (F_g=1 to F_e=2), d(F_g=1 to F_e = 1), e (F_g=2 to F_e=2) and f (F_g=2 to F_e=1). Lines c and d (or e and f) are not well resolved because their separation, 816 MHz, is comparable to the laser line width ~700 MHz and smaller than the pressure-broadened absorption width of the Rb cell ~2.4 GHz.

With a 2 mW/cm^2 pump intensity, the pump rate is ~ 1.6 x 10^4 s^{-1} which is much greater than the Rb spin-exchange rate at 75°C of ~ 4 x 10^2 s^{-1}. A quantitative comparison of magnetometer sensitivity to equations (6.7) and (6.12) has not been made, but the signal for the F_g = 2 line is shown to be larger than that for the F_g = 1 line. The difference is expected to be more pronounced when the magnetometer is used to detect the field of noble gas nuclear moments produced by spin-exchange with Rb. Further work is planned in this direction.

6.3 CONSIDERATIONS FOR FURTHER WORK

A more quantitative comparison of theory and experiment is called for. More importantly, the effect of hyperfine pumping on the Xe nuclear polarization produced by Rb-Xe spin exchange is very interesting and has yet to be investigated.

6.4 REFERENCES

6-1. N.H. Tran, Doctoral Thesis, Columbia University, New York, 1981 (unpublished)

6-2. William Happer, "Optical Pumping", Review of Modern Physics, Vol. 44, p. 169 (1972)

GUIDANCE & CONTROL SYSTEMS
5500 Canoga Avenue, Woodland Hills, California 91365

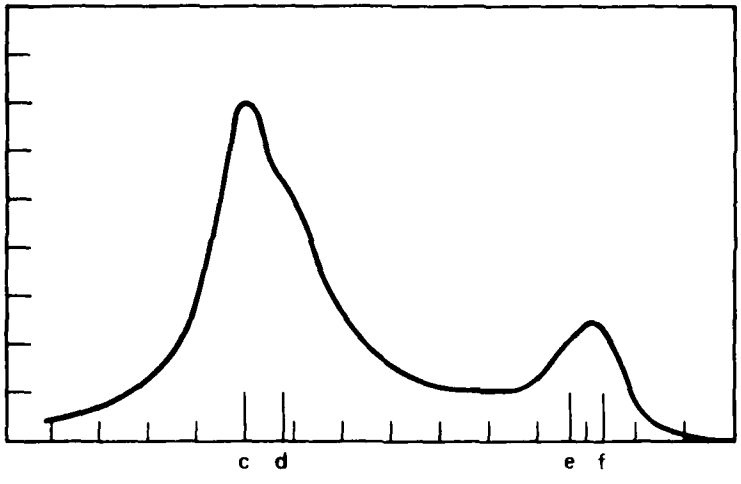

Figure 6-3. Magnetometer Sensitivity

GUIDANCE & CONTROL SYSTEMS
5500 Canoga Avenue, Woodland Hills, California 91365

FSCM 06481

APPENDIX A

DERIVATION OF BASIC EQUATIONS

Litton GUIDANCE & CONTROL SYSTEMS
5500 Canoga Avenue, Woodland Hills, California 91365

APPENDIX A

DERIVATIONS OF BASIC EQUATIONS

Refering again to figure 2-3 the equations at each surface are written in terms of the flux f, crossing that surface and the gradient of polarization S, as

$$N_{Rb}\left(\frac{\partial S}{\partial z}\right)_1 = -\frac{1}{\Delta x \Delta y} Df_1$$

$$N_{Rb}\left(\frac{\partial S}{dz}\right)_2 = -\frac{1}{\Delta x \Delta y} Df_2$$

$$N_{Rb}\left(\frac{\partial S}{\partial x}\right)_3 = -\frac{1}{\Delta y \Delta z} Df_3$$

$$N_{Rb}\left(\frac{\partial S}{\partial x}\right)_4 = -\frac{1}{\Delta y \Delta z} Df_4 \qquad (A.1)$$

$$N_{Rb}\left(\frac{\partial S}{\partial y}\right)_5 = -\frac{1}{\Delta x \Delta z} Df_5$$

$$N_{Rb}\left(\frac{\partial S}{\partial y}\right)_6 = -\frac{1}{\Delta x \Delta z} Df_6$$

where D is the diffusion coefficient. Besides the flux across the boundaries there are also sources and sinks of flux which are caused by the buffer gases f_B, spin exchange f_{ex}, diffusion flux f_d, and the light source f_L. By conservation principles the sum of all flux must equal zero, which gives

$$f1 - f2 + f3 - f4 + f5 - f6 = -f_L + f_{ex} + f_B + f_d \qquad (A.2)$$

Litton GUIDANCE & CONTROL SYSTEMS
5500 Canoga Avenue, Woodland Hills, California 91365
FSCM 06481

Each of the relaxation terms is due to the gas density at the cell temperature, the cross section of collision, the velocity of the particles and the concentration of polarization. The light term, f_L, is proportional to the number of unpolarized atoms of rubidium and the probability of absorption. This provides relations for the sources and sinks of flux as

$$f_B = \frac{N_o P}{P_o} \sigma \bar{v} N_{Rb} VS = k_1 N_{Rb} VS \tag{A.3}$$

$$f_{ex} = \frac{N_o P}{P_o} \sigma \bar{v} N_{Rb} VS = k_2 N_{Rb} VS$$

$$f_L = k_3 N_{Rb} V (1-S) \Phi$$

and

$$f_d = N_{Rb} V \frac{\partial S}{\partial t}$$

Substituting these results and equation A.1 into equation A.2 gives

$$\frac{1}{D} \left[\frac{(\frac{\partial S}{\partial z})_2 - (\frac{\partial S}{\partial z})_1}{\Delta z} + \frac{(\frac{\partial S}{\partial x})_4 - (\frac{\partial S}{\partial x})_3}{\Delta x} + \frac{(\frac{\partial S}{\partial y})_6 - (\frac{\partial S}{\partial y})_5}{\Delta y} \right]$$

$$= -k_3 \Phi (1 - S) + k_1 S + k_2 S + \frac{\partial S}{\partial t} \tag{A.4}$$

Letting Δx, Δy, and $\Delta z \rightarrow 0$ results in

$$\frac{1}{D} \nabla^2 S = KS - k_3 \Phi (1 - S) + \frac{\partial S}{\partial t} \tag{A.5}$$

where

$$K = k_1 + k_2$$

The same thing is done for the light by writing the relationship of light flux λ, in terms of the light intensity Φ, as

$$\lambda_1 = \Phi_1 A$$

$$\lambda_2 = \Phi_2 A \qquad (A.6)$$

where A is the area, $\Delta x \Delta y$. Some light flux is lost as it travels thorugh the volume and is equal to $K_3 f_L$:

$$f_L = \lambda_1 - \lambda_2 = (\Phi_1 - \Phi_2) A \qquad (A.7)$$

Combining (A.7) with f_L from (A.3) gives

$$\frac{\partial \Phi}{\partial z} = k_3 N_{Rb} (1 - S) \Phi \qquad (A.8)$$

Litton GUIDANCE & CONTROL SYSTEMS
5500 Canoga Avenue, Woodland Hills, California 91365

FSCM 06481

APPENDIX B

METHOD FOR COMPUTER SIMULATION

GUIDANCE & CONTROL SYSTEMS
5500 Canoga Avenue, Woodland Hills, California 91365

FSCM 06481

APPENDIX B

METHOD FOR COMPUTER SIMULATOR

B.1 COMPUTER APPROXIMATIONS

The complete system is now described by two simultaneous partial differential equations which are coupled by the light intensity and the polarization.

$$-\frac{1}{D}\nabla^2 S = -\frac{\partial S}{\partial t} + k_3 \Phi (1 - S) - KS \qquad (B.1)$$

and

$$\frac{\partial \Phi}{\partial z} = k_3 N_{Rb} (1 - S) \Phi \qquad (B.2)$$

where

$$K = k_1 + k_2 \qquad (B.3)$$

In the steady state, equation (B.1) becomes

$$-\frac{1}{D}\nabla^2 S = k_3 \Phi N_{Rb} (1 - S) - KS \qquad (B.4)$$

These equations are candidates for solution using finite difference approximations.

First the space inside the cell is divided into a finite difference grid. The size of this grid is determined by the output resolution required and the allowable truncation error. For this problem an equal grid spacing is selected since more resolution in any one particular region of the cell versus any other region of the cell is not required. The steady state solution of this problem is most important since that is the normal operating condition in the gyro. The transient case is of interest to those preforming experiments on cells. For this study the

solution of an elliptic partial differential equation, equation (B.4), is the main concern.

The finite difference approximation for equation (B-4) is written by referring to figure (B.1) and using the central difference of the second derivative, as

$$-\frac{S_1 + S_2 + S_3 + S_4 + S_5 + S_6 - 6\,S_0}{D\,\Delta x^2 \Delta y^2 \Delta z^2} = k_3\,\Phi\,(1 - S_0) - K\,S_0 \qquad (B.5)$$

It is required to find the polarization at point S_0. Solving for S_0 gives

$$S_0 = \frac{S_1 + S_2 + S_3 + S_4 + S_3 + S_6 + Dh^6 k_3\,\Phi}{6 + \Phi\,k_3\,Dh^6 + kDh^6} \qquad (B.6)$$

where,

$$h = \Delta x = \Delta y = \Delta z$$

for a typical grid point. S_1 through S_6 are locations of the six nearest neighbors to point S_0. This equation contains the intensity of the light, Φ, so it is necessary to find an approximation for the light intensity using equation (B.2). Using a forward difference approximation for the first derivative gives

$$\frac{\Phi_8 - \Phi_o}{\Delta z^2} = k_3\,N_{Rb}\,(1 - S_0)\,\Phi_0 \qquad (B.7)$$

and solving for Φ_0 yields

$$\Phi_0 = \frac{\Phi_8}{k_3\,N_{Rb}\,\Delta z^2\,(1 - S_0)} \qquad (B.8)$$

GUIDANCE & CONTROL SYSTEMS
5500 Canoga Avenue, Woodland Hills, California 91365

FSCM 06481

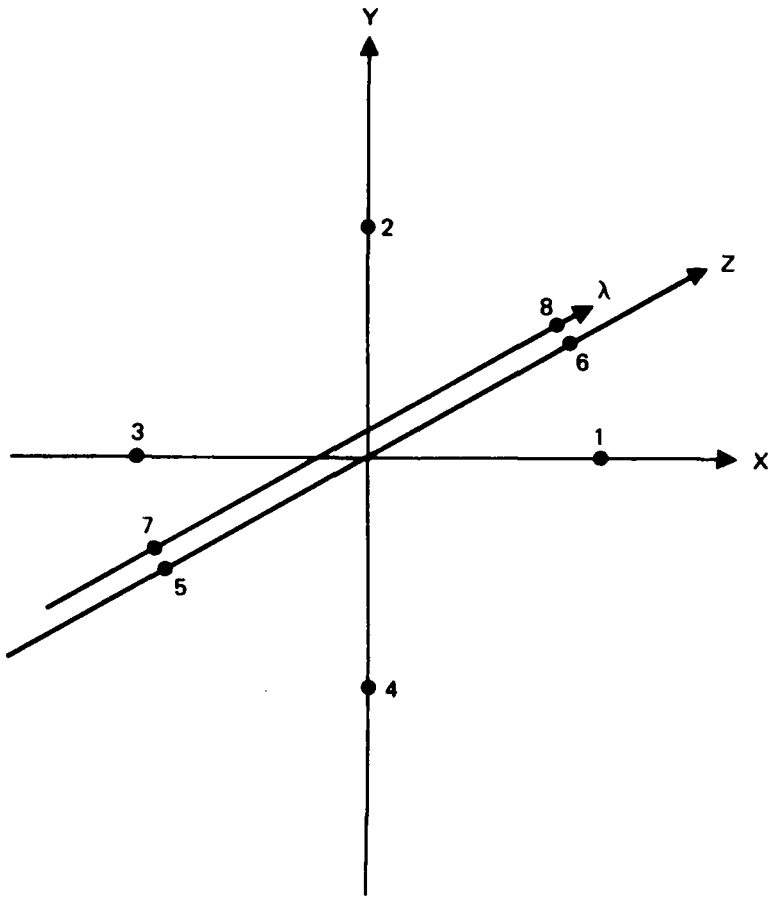

Figure B-1. Finite Difference Grid Used to Determine Approximation of Derivatives

GUIDANCE & CONTROL SYSTEMS
Litton 5500 Canoga Avenue, Woodland Hills, California 91365

The solution of equation (B.1), a parabolic equation, requires an approximation for the first derivative of time. This adds a fourth dimension to the problem which could result in computational instability. For this reason the approximation for the time derivative should be chosen with great care. In addition to solving equation (B.1) it is necessary to use equation (B.8) to obtain the light intensity at each grid point. This leads to the requirement for some sort of iterative approach in the solution. Therefore it is not wise to use an implicit formulation for the time derivative at the same time. One problem with an explicit method is that stability concerns often dictates the size of the time interval. It is preferable to choose the time interval independently. For these reasons and the fact that the solution of equation B.1 is much less important for gyro applications the emphasis is placed on solution of the steady state problem.

The size of the grid spacing for this problem is determined by the resolution of the solution. To help in choosing the best selection for grid spacing it is necessary to consider our expected results. The purpose of optical pumping is to polarize all of the atoms inside the cell (or S = 1). The simulation of this case would require very few points indeed. However, for lower input light intensities, it is expected that the polarization at the front of the cell (towards the light source) would achieve a maximum and decrease in some fashion across the cell. In the worst case, areas of 100 percent polarization and other areas of 0 percent polarization are expected. If only ten points inside the cell along each axis were used, this would equate to a 10 percent resolution of the polarization. One hundred points would give 1 percent resolution. A 1 percent valve probably provides greater resolution than the accuracy of the model. Therefore a selection of 50 points becomes a good compromise based on these concerns and the run time for the selected algorithm.

Truncation errors are related to grid size and the shape of the solution. Using a central difference approximation the largest error term is related to the fourth derivative of the solution. If the solution does not contain a fourth or higher derivative then the truncation error is zero. Varying the intensity of the light source will lead to different distributions of the polarizations. This will cause variations in the truncation error. The truncation error is reduced by using more grid points to solve the problem. By using 50 grid points as explained above and if the solution does not include any irregularities this finite difference approximation is adequate. If this is not true it will become necessary to use more distant neighboring points in the grid to calculate the polarization at point S_0 in figure B-1. This approach results in truncation errors which are proportional to the sixth or eighth derivative.

For this problem the two coupled simultaneous equations (B.5) and (B.6) were solved. The difficulty is that knowledge of the light intensity is needed before calculation of the polarization (and visa-versa). This implies that some sort of iterative technique is required at each point in order to find the light intensity and the polarization at the same time. An added complexity is the three dimensional nature of the problem. To obtain a solution in the shortest amount of time an iterative technique is used to solve for the polarization. The light intensity is a one dimensional problem in the z direction. At the front of the cell the light intensity and the polarization are known. Moving through the cell in the z direction the light intensity at each point in the x-y plane is calculated. Values at the boundary are used to find the polarization of the interior points. This is equivalent to starting at a single point in the x-y plane and then considering circles of increasing radius in the x-y plane progressing along the z axis as shown in figure B-2. It is possible to use an explicit algorithm to solve for the light intensity at each point along the z axis.

GUIDANCE & CONTROL SYSTEMS
5500 Canoga Avenue, Woodland Hills, California 91365

FSCM 06481

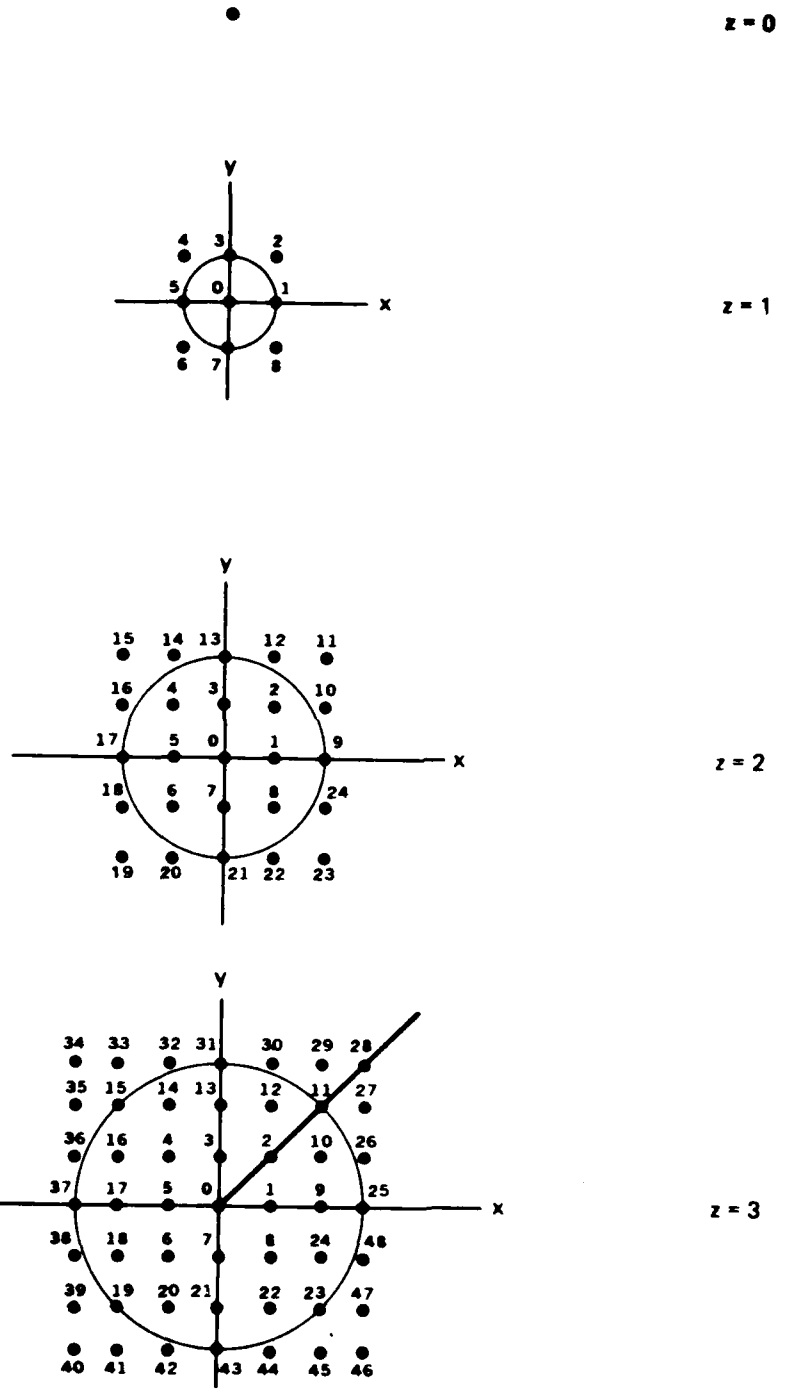

Figure B-2. Cross Sections of the Cell Along the Z Axis Shows Symmetry in the X - Y Plane

The first three cross sections, along the z axis of the cell, are shown in figure B-2 and are arbitrarily numbered for convenience. At z = 1 it is necessary to find the polarization, S, at point 0 based on the values of polarization at points 1, 3, 5, and 7, knowing the boundary condition for S. Φ at point 0 is evaluated first. The intensity at all other points is at its initial value. It is then possible to find the value of S at point 0 directly knowing the values at point 0 with z = 0.

Moving down the z axis, for example at z = 2, Φ is known at points 9, 13, 17, 21 and its value at points 1, 2, 3, 4, 5, 6, 7, and 8 is needed. The polarization, S, is known only at points 9, 13, 17, and 21. Using a guess of both the intensity and polarization at the interior nine points it is possible to iterate to the final values by knowing the values of Φ and S at the z = 1 level. Because of the circular geometry, calculation of the values only in the first quadrant is required. The problem is reduced to finding the values of Φ and S at points 0, 1, 2, and 3. Any point on the x or y axis has 2 neighbors which are the same value and this also simplifies the calculations. Further, because of symmetry each point in the grid has neighbors which have the same value because of their location with respect to the boundary. The values of Φ and S in only 1/2 a quadrant are actually needed. The complexity of this problem is significantly reduced using symmetry.

Taking a central difference at each point means that the values of Φ and S on the z = 2 level are determined by the values on the z = 1 level. Many of the points of the grid fall outside the sphere thus further reducing the number of calculations.

The best iterative algorithm for solving for the polarization is the successive overrelaxation method. The problem with this method, however, is the determination of the relaxation factor ω, which lies between 1 and 2. With ω equal to 1 or 2 this method

reduces to the Gauss - Seidel method. The value of this factor is not known beforehand; it is only found experimentally. This problem could run with a few points at first and with different values for ω in order to monitor how many cycles of iteration are required for a solution. A solution exists when the difference between the current value at a point and the value at that point during the previous iterative cycle is less than the required tolerance.

To solve this problem for the transient case it is necessary to repeat this whole process at each time level using the previous time level or backward difference to approximate the time derivative.

Because of symmetry this problem is reduced to fewer calculations than first anticipated and the selection of other algorithms is possible. Using the successive overrelaxation method, however, is the best choice because of speed of operation. The solution of this entire problem is actually a Crank - Nicolson technique when dealing with the two coupled equations in order to find a solution.

It is possible to make some interesting predictions about computer run time and storage. For a 50 point problem to store the entire array would require 125 K words of memory. This is not a large amount for a modern computer. But with symmetry and spherical boundary conditions this requirement is reduced to about 24 K. At each point there are eight arithmetic operations and using 6 microseconds per operation (for a VAX 780) it will take approximately 4 seconds per iteration. The number of iterations depends on many factors. Setting ω equal to 1, or in other words using the Gauss - Seidel method, a certain number of iterative cycles is expected. However, for an optimum choice of ω one tenth that number of cycles is needed.

Writing the actual computer program is straightforward and a flow chart is shown in figure B-3. The process is started by reading in the values of a tolerance on the iterative cycle, TOL, along with the number of points in the grid, M, and the parameters for the problem. For the first cycle the intensity Φ is set equal to Φ_o and S at the boundary equal to the polarization at the wall. Proceeding along the z axis the intensity, Φ, and polarization, S, in each of the x-y planes is found. These calculations are repeated for each value of z until the end of the cell is reached. Checking the error term reveals whether the iteration is complete, and these iterative cycles are repeated until the error is acceptable. The detailed calculation of Φ or S are not shown in the flow chart because of the availability of standard software packages for these specific algorithms.

GUIDANCE & CONTROL SYSTEMS
5500 Canoga Avenue, Woodland Hills, California 91365

FSCM 06481

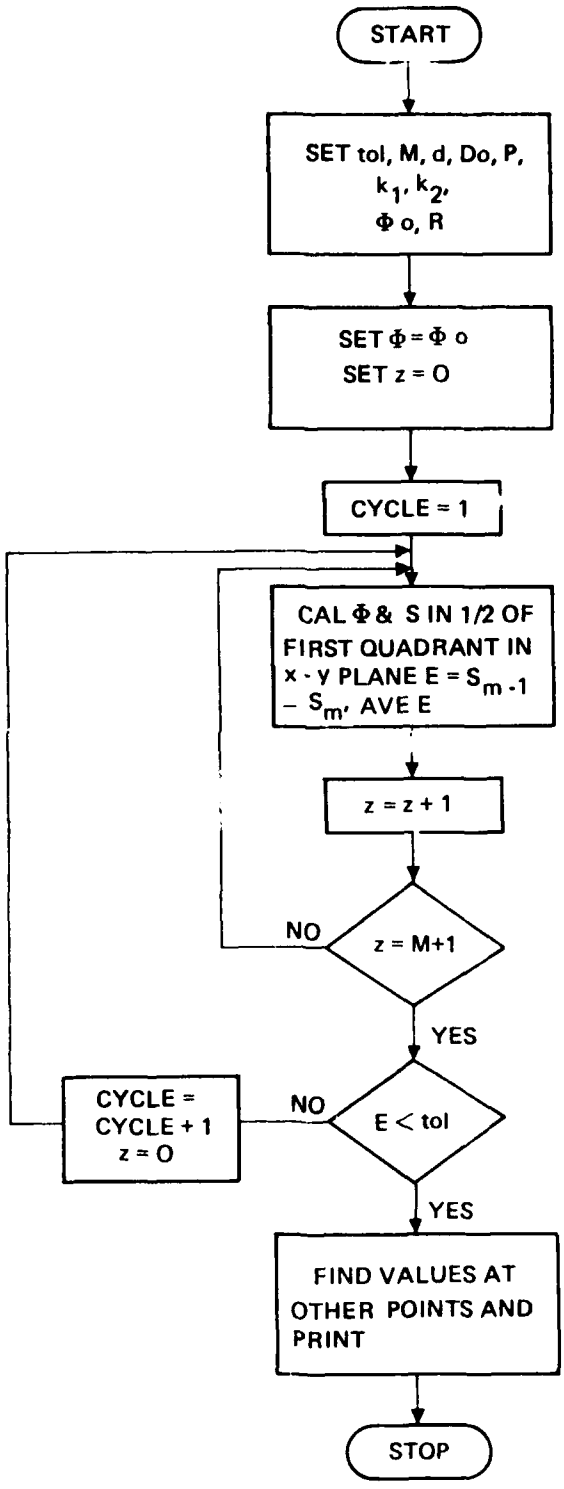

Figure B-3. Computer Solution Uses Implicit Methods